JGR Oceans

RESEARCH ARTICLE
10.1029/2024JC021624

Physical Drivers of a Massive Harmful Algal Bloom in the Northern Bering and Chukchi Seas in Summer 2022

L. S. Lago[1], R. S. Pickart[1], P. Lin[2], F. Bahr[1], E. Fachon[1], M. L. Brosnahan[1], M. Pathare[1], E. Muhlbach[3], K. Horn[1], A. Rajagopalan[1,4], and D. M. Anderson[1]

[1]Woods Hole Oceanographic Institution, Woods Hole, MA, USA, [2]School of Oceanography, Shanghai Jiao Tong University, Shanghai, China, [3]Florida Fish and Wildlife Conservation Commission - Fish and Wildlife Research Institute, St. Petersburg, FL, USA, [4]College of Science, Northeastern University, Boston, MA, USA

Abstract In summer 2022 the Chukchi Sea exhibited the highest concentrations of the toxin producing dinoflagellate *Alexandrium catenella* ever recorded in the Arctic, documented by two back-to-back cruises. Here, we use the shipboard hydrographic and velocity data, together with ocean reanalysis fields, to investigate the physical factors that helped dictate the initiation and evolution of the bloom. High concentrations of *Alexandrium catenella* vegetative cells were first detected west of St. Lawrence Island, within Bering Summer Water, and were subsequently advected poleward. A backward trajectory calculation indicates that the water transporting the bloom originated from the Gulf of Anadyr, then passed through Anadyr Strait and the US side of Bering Strait, reaching 71°N roughly a month and a half later. A strong southerly wind event diverted part of the bloom into Kotzebue Sound and caused it to mix with warmer Alaskan Coastal Water, further promoting cell growth. We also investigate the possibility that part of the bloom was generated locally in the Ledyard Bay region due to germination from the large cyst bed there, as was observed in summer 2018. While such local germination may have occurred in early August, as was the case in 2018, considerably colder near-surface temperatures in 2022 would have slowed vegetative cell growth relative to conditions in 2018. Using mooring data from the Bering Strait we demonstrate that the heat flux through the strait largely dictates the timing of cyst germination in the Ledyard Bay region, and also shapes subsequent growth and accumulation of vegetative cells there.

Plain Language Summary Harmful algal blooms (HABs) are an emerging threat to the ecosystem and coastal communities of the Pacific sector of the Arctic Ocean. In summer 2022, a large toxic HAB was documented in the northern Bering Sea and southern Chukchi Sea during back-to-back survey cruises. Here we use shipboard data, plus ocean numerical model fields, to investigate the spreading and evolution of the bloom. We demonstrate that the water carrying the bloom, and the bloom population itself, likely emanated from the Gulf of Anadyr, and then progressed northward through Anadyr Strait and the US side of the Bering Strait into the Chukchi Sea. Strong winds from the south caused part of the bloom to penetrate eastward into Kotzebue Sound, close to the Alaskan coast. We also investigate the possibility of a locally generated HAB farther north in the Ledyard Bay region due to germination of cysts present in huge abundance in the sediments there. We demonstrate that the timing of such germination is strongly dictated by the temperature of the bottom water flowing northward through the Bering Strait, and that the growth rate of the resulting vegetative cells is influenced by the temperature of the near-surface water flowing northward through the strait.

Key Points:

- The hydrographic factors dictating the evolution of a massive harmful algal bloom in the Northern Bering and Chukchi Seas are investigated
- The *Alexandrium catenella* bloom likely originated in the Gulf of Anadyr, passed through Anadyr and Bering Strait toward the Chukchi Shelf
- Interannual variability of heat transport through Bering Strait influences the bloom development in northern waters

Supporting Information:

Supporting Information may be found in the online version of this article.

Correspondence to:

L. S. Lago,
loreley.lago@whoi.edu

Citation:

Lago, L. S., Pickart, R. S., Lin, P., Bahr, F., Fachon, E., Brosnahan, M. L., et al. (2025). Physical drivers of a massive harmful algal bloom in the Northern Bering and Chukchi Seas in summer 2022. *Journal of Geophysical Research: Oceans*, *130*, e2024JC021624. https://doi.org/10.1029/2024JC021624

Received 22 JUL 2024
Accepted 7 APR 2025
Corrected 24 MAY 2025

This article was corrected on 24 MAY 2025. See the end of the full text for details.

Author Contributions:

Conceptualization: L. S. Lago, R. S. Pickart
Data curation: F. Bahr, M. L. Brosnahan, M. Pathare, E. Muhlbach, K. Horn, A. Rajagopalan
Formal analysis: L. S. Lago, R. S. Pickart, P. Lin
Funding acquisition: R. S. Pickart, D. M. Anderson
Investigation: L. S. Lago, R. S. Pickart, P. Lin
Methodology: L. S. Lago, E. Fachon
Project administration: R. S. Pickart, P. Lin, D. M. Anderson
Resources: R. S. Pickart
Supervision: R. S. Pickart, P. Lin
Validation: L. S. Lago, F. Bahr

1. Introduction

The Chukchi Sea, a marginal sea of the Pacific Arctic located north of the Bering Strait, is among the most biologically productive areas of the world ocean (Grebmeier, 2012). It also plays a key role in Arctic amplification, as it is a source of heat to the atmosphere during the summer and fall due to the warm water input from the Bering Sea (Danielson et al., 2020). The main source of heat to the Chukchi Sea is through Bering Strait (Woodgate, 2018), and different studies have investigated the poleward advection of this heat across the shelf (e.g., Weingartner et al., 1998). Using data from an extensive array of moorings on the shelf in 2013–2014, Tian et al. (2021) demonstrated a clear poleward advective signal of warm near-bottom temperatures from Bering Strait at the onset of the summer season.

Despite the prevailing northeasterly winds, the mean circulation on the Chukchi shelf is poleward, topographically steered (Weingartner et al., 2005), and driven by the large-scale pressure gradient between the Pacific and

Visualization: L. S. Lago, R. S. Pickart, P. Lin
Writing – original draft: L. S. Lago
Writing – review & editing: L. S. Lago, R. S. Pickart, P. Lin, F. Bahr, E. Fachon, E. Muhlbach, A. Rajagopalan, D. M. Anderson

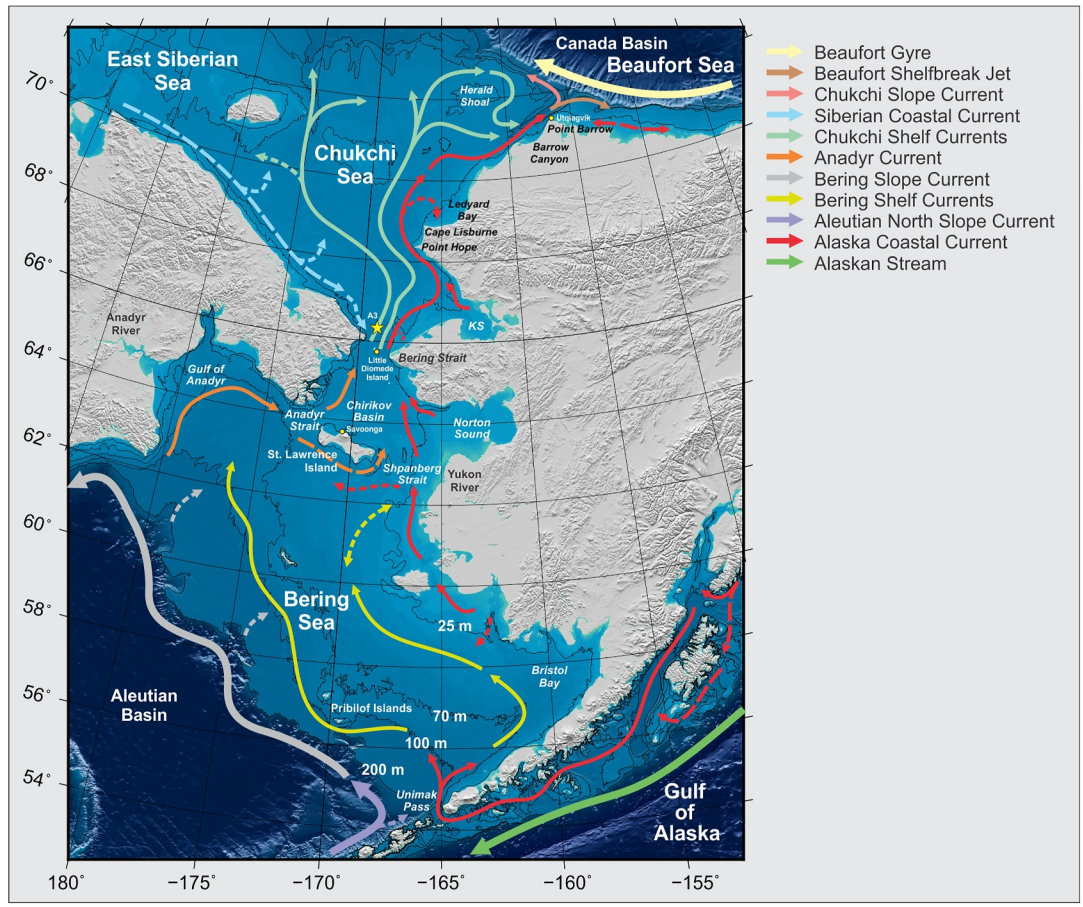

Figure 1. Schematic circulation and place names in the Bering and Chukchi Seas, adapted from Danielson et al. (2022).

the Arctic (Coachman & Aagaard, 1988; Stigebrandt, 1984). North of Bering Strait the Pacific-origin water follows three main branches (Figure 1): the western branch, the Central Channel branch (CC), and the Alaskan Coastal Current (ACC). The western branch, emanating from the western channel of Bering Strait (west of the Diomede Islands), carries salty, nutrient-rich waters primarily from the Gulf of Anadyr (Coachman & Aagaard, 1988; Pickart et al., 2010). The other two branches enter the Chukchi Sea via the eastern channel of Bering Strait (east of the Diomede Islands): the CC carries a mixture of Anadyr Water and central Bering shelf water (Weingartner et al., 2005), and the ACC advects very warm and fresh water originating from continental discharge in the Gulf of Alaska (Paquette & Bourke, 1974). All of the water masses and currents passing through Bering Strait have a strong seasonal component and are influenced by local winds (Lin et al., 2019; Pisareva et al., 2015; Weingartner et al., 2005; Woodgate et al., 2005, 2012) as well as remote winds (Danielson et al., 2014).

The Anadyr Water, as well as the cold, dense winter water formed in the northern Bering and Chukchi Seas, are rich in nutrients (Arrigo et al., 2017; Muench et al., 1988; Pacini et al., 2019). These nutrients support phytoplankton blooms starting in the spring, when light availability increases. The recent loss of sea ice and warmer water conditions in spring have led to higher primary productivity in open water. Using an ocean color algorithm parameterized for the Arctic Ocean, Lewis et al. (2020) documented a 57% increase in primary production between 1998 and 2018. Thinning of the sea ice, together with the presence of melt ponds, has led to the occurrence of under-ice blooms (Arrigo et al., 2012, 2014; Lowry et al., 2014; Pickart et al., 2024). Notably, one of the largest phytoplankton blooms ever recorded globally occurred on the northern Chukchi shelf under a meter of consolidated pack ice (Arrigo et al., 2012).

One of the phytoplankton species responsible for harmful algal blooms (HABs) worldwide is the dinoflagellate *Alexandrium catenella*, which produces paralytic shellfish toxins (PSTs), some of the most potent toxins among

the HAB toxin families (Anderson et al., 2012). *A. catenella* has been thoroughly studied in several regions of the world, including the Gulf of Maine (e.g., Anderson, 2014; Anderson et al., 2005; Li et al., 2020), the Mediterranean Sea (Bravo et al., 2008), Chile (Mardones et al., 2016), and the eastern coast of Tasmania (Condie et al., 2019). Historically, the Pacific Arctic has been considered too cold for these organisms to form recurring blooms. However, both locally originating and remotely advected blooms of *A. catenella* have recently been documented in the Chukchi Sea (Anderson, Fachon, et al., 2021; Fachon et al., 2025; Natsuike, Oikawa, et al., 2017). The local source of *A. catenella* north of the Bering Strait is likely a large bed of resting cysts in the sediments, located in the Ledyard Bay region (Anderson, Fachon, et al., 2021; Natsuike et al., 2013). These studies demonstrated that bottom water temperatures can now become warm enough to support relatively rapid germination of the cysts, which, in the presence of sufficient nutrients and warm surface waters, would lead to a locally generated bloom. In addition to this Arctic cyst population, the Bering Sea represents a remote source of *A. catenella* to this region. Cells originating in the Bering Sea can be transported northward into the Chukchi Sea through the Bering Strait (Anderson, Fachon, et al., 2021; Fachon et al., 2025; Natsuike et al., 2013).

In light of the increasing ocean temperatures throughout the water column (Danielson et al., 2020; Wood et al., 2015) and more frequent and more intense marine heat waves in the last decades related to ice retreat in the region (Carvalho et al., 2021; Hu et al., 2020), it seems plausible that HAB activity in the western Arctic Ocean will continue to increase. An enhanced presence of *A. catenella*, whose toxins are transferred across trophic levels, would threaten not only the local marine ecosystem (Anderson, Fensin, et al., 2021; Lefebvre et al., 2016; Shearn-Bochsler et al., 2014) but also the coastal, largely indigenous, communities that depend on subsistence harvesting. It is thus vital to understand the dynamics of HABs in the Pacific Arctic, including the role of ocean currents, sea ice, and atmospheric forcing.

In summer 2022, the highest concentrations ever recorded of *A. catenella* in the Chukchi Sea were detected during two back-to-back cruises spanning from mid-July to early September (Fachon et al., 2025). The bloom was first detected in the northern Bering Sea and subsequently progressed through the Bering Strait, after which it reached its peak concentration in the Kotzebue Sound region. This paper explores the roles of different physical drivers in the initiation and spread of the 2022 advected HAB event. While the general northward progression of the bloom was expected and has been previously described (Fachon et al., 2025), there are numerous aspects of its evolution that require further explanation, including its water mass composition, detailed trajectory, the impacts of circulation and wind forcing, and whether there was a contribution from local germination via the cyst bed in the Ledyard Bay region. This paper addresses these aspects.

2. Data and Methods

2.1. In-Situ Measurements

During summer 2022, two back-to-back cruises were carried out on R/V *Norseman II* in the northern Bering Sea, eastern Chukchi Sea, and western Beaufort Sea. Figure 2 shows the location of the sections occupied during both cruises. The first cruise (NRS2022-01S), henceforth referred to as LEG 1, was carried out from 19 July to 15 August and encompassed the region from St. Lawrence Island to Barrow Canyon. This leg focused primarily on evaluating the distribution and dynamics of HAB species, with a focus on *A. catenella*. Many of the transects chosen were repeat occupations of standard sections, including Distributed Biological Observatory lines 1–5 which are occupied regularly by the international community. Note that the DBO1 and DBO2 lines were variations of the official versions found at https://www.pmel.noaa.gov/dbo/. The second cruise (NRS2022-02S), henceforth referred to as LEG 2, was carried out from 17 August to 6 September. This leg focused more on biogeochemical sampling with less extensive HAB measurements. Some of the sections were the same as in LEG 1, but, due to the shorter duration of the cruise, the geographical coverage was reduced. Due to the desire to sample the last of the winter water on the Chukchi shelf, the DBO4 and DBO5 sections were extended toward the northwest to the shelfbreak. Also, due to the continued meltback of the pack ice, we were able to occupy an additional section in open water in the western Beaufort Sea. Finally, a section along the US/Russian convention line was occupied with an unprecedented horizontal resolution of 20 km.

2.1.1. Hydrographic Data

A total of 196 (LEG 1) and 239 (LEG 2) conductivity-temperature-depth (CTD) stations were completed using a Sea-Bird Scientific 911+ system mounted on rosette with 12 10-L Niskin bottles. The measurements included

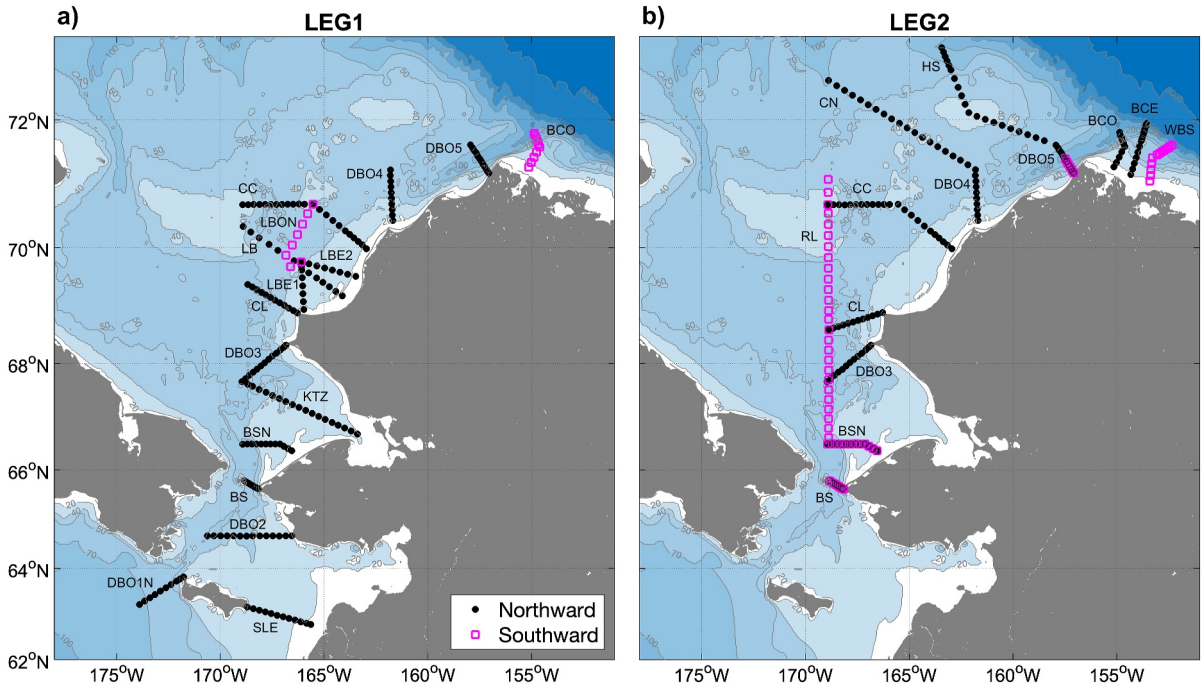

Figure 2. Sections occupied during (a) LEG1 and (b) LEG2 of the *Norseman II* cruise. The stations occupied during the northbound sampling are in black and during the southward sampling in magenta. The bathymetry is from ETOPOv2. The acronyms of the sections are: SLE = Saint Lawrence island; DBO1N = Distributed Biological Observatory (DBO) 1 North; DBO2 = Distributed Biological Observatory 2; BS = Bering Strait; BSN = Bering Strait North; KTZ = Kotzebue; DBO3 = Distributed Biological Observatory 3; CL = Cape Lisburne; LBE1 = Ledyard Bay East 1; LBE2 = Ledyard Bay East 2; LB = Ledyard Bay; LBON = Ledyard Bay outer North; CC = Central Channel; DBO4 = Distributed Biological Observatory 4; DBO5 = Distributed Biological Observatory 5; BCO = Barrow Canyon Outer; HS = Hanna Shoal; BCE = Barrow Canyon East; WBS = Western Beaufort Sea; and RL = Russian Line.

dual temperature and conductivity, dissolved oxygen, fluorescence, beam transmission, and photosynthetically active radiation. The temperature and conductivity sensors were calibrated at Sea-Bird prior to the cruise, and the accuracy of the temperature measurement is deemed to be 0.001°C. For conductivity, we collected salt samples on two ~1,000 m casts on LEG 2 in order to check for a qualitative offset of the sensors. While this is not enough information to perform a robust conductivity calibration, there was excellent agreement between the CTD conductivity values and the bottle values. Based on this, we estimate the accuracy of the CTD salinity to be 0.009 (practical salinity). Final 1-dbar averaged downcast files were created using Sea-Bird Scientific processing scripts. For all analyses presented below, we use potential temperature and potential density referenced to the sea surface, hereafter referred to simply as temperature and density.

2.1.2. Velocity Data

Velocity was measured on both legs using R/V *Norseman II's* Teledyne RD Instruments (TRDI) WH300 (300 kHz) hull-mounted acoustic Doppler current profiler (ADCP). The acquisition and processing were done using TDRI's VMDAS software. During the week-long transit from the ship's home port to the start of LEG 1, the performance of the system was checked and any adjustments to the calibration were applied. At regular intervals during the cruise, typically after the completion of a section, pre-processed data (.LTA files) were sent ashore for additional processing and quality control. Using the CODAS software package from the University of Hawaii (https://currents.soest.hawaii.edu), we removed remaining "sub-bottom" data—a common feature when processing VMDAS data—and also addressed occasional ADCP noise during rough sea states. Lastly, we used the TPXO9v3 tidal model (http://volkov.oce.orst.edu/tides; Padman & Erofeeva, 2004) to remove the barotropic tidal signal from each profile.

2.1.3. Imaging FlowCytobot Data and Underway Hydrographic Data

Measurements of *A. catenella* cell concentration in near-surface waters were collected continuously throughout both legs using an Imaging FlowCytobot (IFCB, McLane Laboratories). The IFCB is a submersible automated

imaging flow cytometer (Olson & Sosik, 2007) designed to image suspended particles ranging in size from 10 to 150 μm. It has been used widely to characterize phytoplankton communities, and, specifically, to assess HABs (e.g., Proenca & Hallegraeff, 2017) including *A. catenella* (Brosnahan et al., 2015, 2017). The IFCB was set up to sample from an underway flow-through seawater system (intake depth of approximately 3 m) aboard the *Norseman II*, generating imagery of the phytoplankton community (Fachon et al., 2025). The IFCB processed and imaged several 5 mL samples every hour, with image acquisition triggered by chlorophyll fluorescence (PMTB). A convolutional neural network classifier was used to sort images into groups, mostly to the genus level, and the output of this classifier was further refined by manual annotation of all *A. catenella* cells. Cell concentration was calculated by normalizing cell counts to the sample volume. The timestamp of each sample was used to pair underway temperature and salinity data from the *Norseman II's* thermosalinograph (TSG, SBE21). Underway TSG data were validated against the CTD near-surface measurements. This comparison revealed a consistent offset between the CTD and TSG measurements across both cruise legs: TSG readings were slightly higher in temperature ($+0.17 \pm 0.14$°C) and lower in salinity (-0.46 ± 0.09) than co-occurring CTD readings. Accordingly, these corrections were applied to the TSG data set.

2.2. Historical Velocity Measurements

For part of the analysis, we use velocity data from a newly compiled database of shipboard ADCP measurements covering the Chukchi shelf for the period 2002–2023, known as ChukSA (https://scienceweb.whoi.edu/seasoar/chukchi_sadcp). The climatology consists of data collected during 56 cruises, primarily between July and September. All the data were subject to careful inspection and quality control, after which the TPXO9v3 tidal model was used to remove the barotropic tidal signal. For more detailed information, see Pickart et al. (2023). These data were used for the analysis of the wind effect on the shelf currents in the Kotzebue Sound region (Section 3.2).

2.3. Ocean Reanalysis Fields

GLORYS12v1 is a global ocean eddy-resolving reanalysis distributed by the Copernicus Marine Environment Monitoring Service (CMEMS, https://doi.org/10.48670/moi-00021). It has a 1/12° horizontal resolution (∼8 km) and 50 standard vertical levels at different vertical resolutions. The shallowest 10 m of the water column has a ∼1 m resolution, and below this the resolution starts decreasing; for example, at 100 m depth the vertical resolution is ∼15 m. This product is available from 1993 onward. It is based on the Nucleus for European Modeling of the Ocean (NEMO) model, forced at the surface by the ECMWF ERA-Interim reanalysis (1993–2018) and the ERA5 reanalysis (2018-present). It assimilates satellite observations of sea level anomaly, sea surface temperature, sea ice concentration, and in-situ observations of temperature and salinity vertical profiles.

Here we consider the daily products of temperature and horizontal velocity. Lin et al. (2023) previously validated the reanalysis velocities with mooring observations in the vicinity of Bering Strait. We carried out a comparison between bottom temperature reanalysis data in the Ledyard Bay region and in-situ measurements from the historical hydrographic data set of Lin et al. (2021) covering the period 2003–2018. A box was defined for the cyst bed in the Ledyard Bay region (shown below in Figure 5), and, for every in-situ hydrographic profile within the box, we interpolated the GLORYS12v1 gridded data to the location of the profile. The average temperature over the bottom 5 m of all the profiles were then regressed against the interpolated reanalysis bottom temperatures (Figure S1 in Supporting Information S1). This showed good agreement with an R^2 of 0.85 and a linear regression slope of 0.96, with a small offset of 1.16°C. We used this linear regression to adjust the GLORYS12v1 bottom temperatures in the Ledyard Bay region.

2.4. Atmospheric Reanalysis Fields

To address the atmospheric forcing, we use the European Center for Medium-Range Weather Forecasts (ECMWF, https://www.ecmwf.int/) ERA5 10 m wind product. It is an hourly product with a spatial resolution of 1/4°, covering the period from 1940 to the present (Hersbach, 2016).

2.5. Water Mass Analysis Using the Potential Density—Potential Spicity Framework

In order to classify the different water masses, it is advantageous to work in potential density—potential spicity (σ_0–π_0) space. Since these two variables (both referenced to the sea surface) are orthogonal to each other, and the

magnitude of their gradients are comparable (e.g., Huang et al., 2020), the σ_0–π_0 framework is suitable for estimating how close a water parcel is to the three endmembers of a mixing triangle, where each endmember represents 100% of the associated water mass. Using the calculated σ_0–π_0 distances to each end member, we determine the percent contribution of that endmember to the water parcel in question. We verified that our chosen endmembers are physically meaningful by comparing their temperature and salinity values to historical data from the respective source regions.

2.6. Particle Advection Analysis

A particle advection analysis was carried out using the GLORYS12v1 reanalysis daily velocity fields. The trajectories of particles were computed backwards in time, from the point of arrival. This analysis was carried out by applying the Ocean Parcels package in Python (https://oceanparcels.org/) to the near surface velocities at 13 m depth.

2.7. Heating Degree Days and Growth Rate

In the context of cyst germination, heating degree days (DD) are calculated as the integral of daily temperature with respect to time once the water has reached a defined threshold, in this case 0°C (Fischer et al., 2018). While there is some variability in the DD required for germination of *A. catenella* cysts, laboratory experiments on *A. catenella* populations from different geographical regions, including the Chukchi Sea, show a broad consistency in DD requirements for this species, with a mean of approximately 85 DD required for cyst germination (Anderson, Fachon, et al., 2021). This implies, for example, that water at 1°C would result in 50% germination after 85 days, while in 10°C water, it would take 8.5 days.

As a way to examine the changing growth conditions related to near-surface temperatures, we applied a fourth degree polynomial fit to the available measurements of growth rate (GR) of *A. catenella* versus temperature measured in cultured Chukchi Sea isolates (values reported in Anderson, Fachon, et al., 2021, Supporting Information). The following equation expresses the polynomial fit:

$$\mathrm{GR}(T) = -4.7\ 10^{-7}\ T^4 - 1.3\ 10^{-4}\ T^3 + 2\ 10^{-3}\ T^2 + 2.9\ 10^{-2}\ T - 8.1\ 10^{-2}$$

In particular, we computed the GR along the pathways based on the GLORYS12v1 reanalysis fields at 13 m depth. The results are presented as divisions per day; that is, a value of 0.5 divisions day^{-1} implies that, in the absence of external pressures such as grazing and in the presence of sufficient nutrients, a population requires 2 days to double.

2.8. Heat Transport Estimate

The heat transport is given by

$$\mathrm{HT} = \int \rho\ C_w\ (T - T_{\mathrm{ref}})\ v\ dA,$$

where C_w is the specific heat capacity (3,900 J kg^{-1} K^{-1}), ρ is the background density (1,023 kg m^{-3}), T_{ref} is the reference temperature (taken to be the freezing point, −1.9°C, following previous studies), v is the cross-section velocity, T is the temperature, and A is the cross-sectional area.

3. Results

3.1. Water Mass Distribution in Summer 2022

During the two cruises in summer 2022, the *Norseman II* occupied over 400 CTD stations, enabling a rigorous description of the summer water mass distribution of the region that sheds important light on biological processes such as HABs. During the two cruises, there were both summer and winter waters present in the study domain. To characterize this, we use a set of water mass definitions that have been adopted in numerous previous studies (e.g., Pickart et al., 2023; limits shown in Figure 3). The two types of summer water are Alaskan Coastal Water (ACW), which stems from continental runoff, and Bering Summer Water (BSW), which is a mixture of central Bering

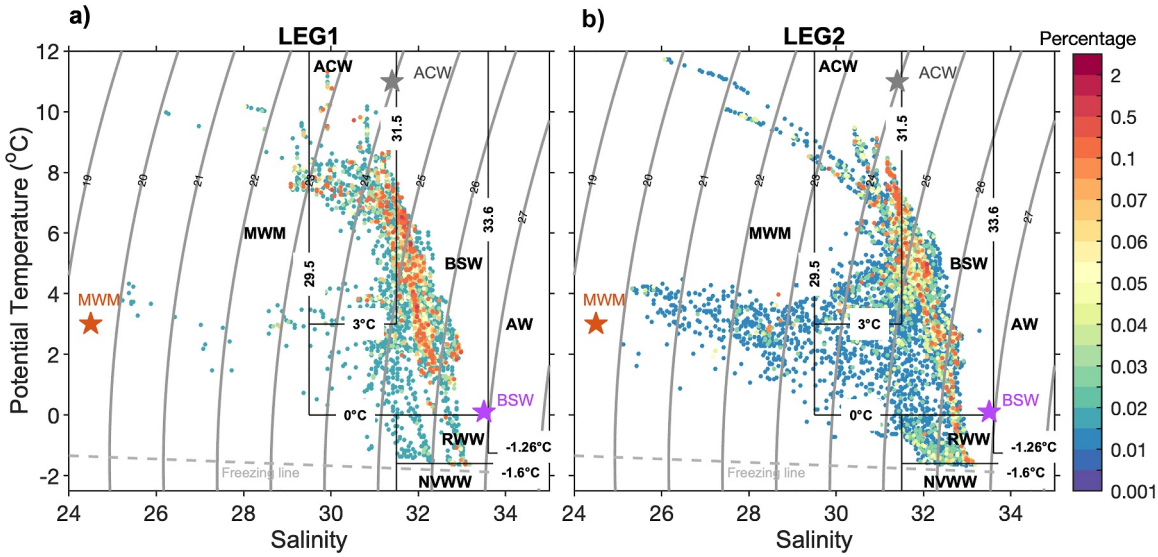

Figure 3. Temperature-Salinity diagram for all the stations occupied during (a) LEG 1 and (b) LEG 2 for the shallowest 35 m of the water column. The colors represent the percent occurrence of water within 0.05°C temperature × 0.05 salinity bins. The contours are dense. The Black lines denote the water mass boundaries. ACW = Alaskan Coastal Water; BSW = Bering Summer Water; MWM = Melt water/Meteoric water; NVWW = New Ventilated Winter Water; RWW = Remanent Winter Water; and AW = Atlantic Water. The chosen end-members for the ACW, BSW, and MWM are indicated by the gray, purple, and orange stars, respectively.

shelf water and Anadyr Water. The two types of winter water are Newly Ventilated Winter Water (NVWW), which was formed the previous winter on the northern Bering and Chukchi shelves (Muench et al., 1988; Pacini et al., 2019), and Remnant Winter Water, which is NVWW that has been warmed due to solar heating and mixing with warmer summer waters (Gong & Pickart, 2015). Sea-ice melt water and meteoric water were also present in the study area. These are considered as a single water type (MWM). Finally, Atlantic Water (AW) was present at depth at stations on the continental slope. It is important to note that the areas covered by each leg are different; LEG 1 includes the Bering Sea region near St. Lawrence Island, and LEG 2 extends to the northern Chukchi shelf.

There was a clear delineation of the water masses by depth (Figure S2 in Supporting Information S1). Shallow waters above 30 m depth are predominantly composed of the summer waters ACW and BSW, along with MWM. Below 30 m depth resides the saltier portion of BSW along with the two types of winter water and AW. The vertical distribution of *A. catenella* from the Niskin bottle samples (not shown), reveals that the highest concentrations are found in the shallow waters, with cell concentrations exceeding 5,000 cells L^{-1} above 30 m depth. Hence, in the following analysis we focus on the shallow summer waters ACW and BSW, and MWM. To determine the depth of the transition between the summer waters and the deeper winter waters we computed the Brunt-Vaisala frequency at each station, an indicator of the vertical stratification, and determined the maximum depth of the pycnocline. On average this was found to be 35 m.

The temperature-salinity (T-S) diagrams for the shallowest 35 m of the water column for each leg of the cruise reveal that the dominant water masses are ACW and BSW (Figure 3), with a large amount of water near the boundary of the two (keep in mind that the chosen water mass boundaries are somewhat subjective). The difference between the two legs is not only temporal, but also related to the spatial coverage of the occupied sections. LEG 1 shows higher occurrence of ACW, consistent with the more extensive sampling in the eastern part of the domain where the ACC flows. During LEG 2, BSW is found over a wider range of salinities, and MWM is more prevalent because more sections were occupied north of 69°N closer to the retreating ice edge.

As described in Section 2.5, an analysis in σ_0–π_0 space was used to characterize the different water masses in the study domain. We chose three endmembers that represent pure ACW, BSW, and MWM, respectively. These are seen in T-S space in Figure 3 and in σ_0–π_0 space in Figure S3 in Supporting Information S1 (see also Table 1). Figure S3 in Supporting Information S1 shows the percentage axes for the respective endmembers used to quantify the makeup of a given water parcel. We computed the vertical average of water mass percentage between 0 and 35 m depth at each station occupied during the two legs. The resulting lateral distributions of these percentages are shown in Figure 4 for the northward portion of LEG 1. As expected, ACW dominates the eastern

Table 1
Temperature (T), Salinity (S), Potential Density (σ_0), and Potential Spicity (π_0) Values for the Three Endmembers Chosen to Represent the ASW, BSW and MWM

	T (°C)	S	σ_0 (kg m^{-3})	π_0 (kg m^{-3})
ACW	11.0	31.4	24.0	−2.5
BSW	0.1	33.5	26.9	−3.2
MWM	3.0	24.5	19.5	−3.4

boundary region from the Bering Sea to approximately 69°N near Cape Lisburne. North of there, the percentage of BSW is higher near the coast, which likely reflects the seasonal presence of the ACC; that is, this early in the season the ACC has not fully reached these northern latitudes.

The lateral distribution of BSW is also largely as expected. In particular, the percentages tend to be higher on the western ends of the sections. The percentages are especially high south of the Bering Strait on the western side of St. Lawrence Island and on the Russian side of the Chirikov Basin, where the presence of Anadyr Water is expected to be dominant. Two other locations of high BSW presence are the offshore end of the DBO3 line (where it meets the KTZ line) and in the Central Channel (the offshore ends of the CC and LB lines). With regard to the former, this is a region of enhanced benthic biomass (Grebmeier et al., 2015, 2018) which is reflective of high-nutrient Anadyr Water. MWM shows the lowest percentages among the three water masses. However, the relative percentages are higher on the eastern ends of the SLE and DBO2 lines in the Bering Sea, which is a signature of continental

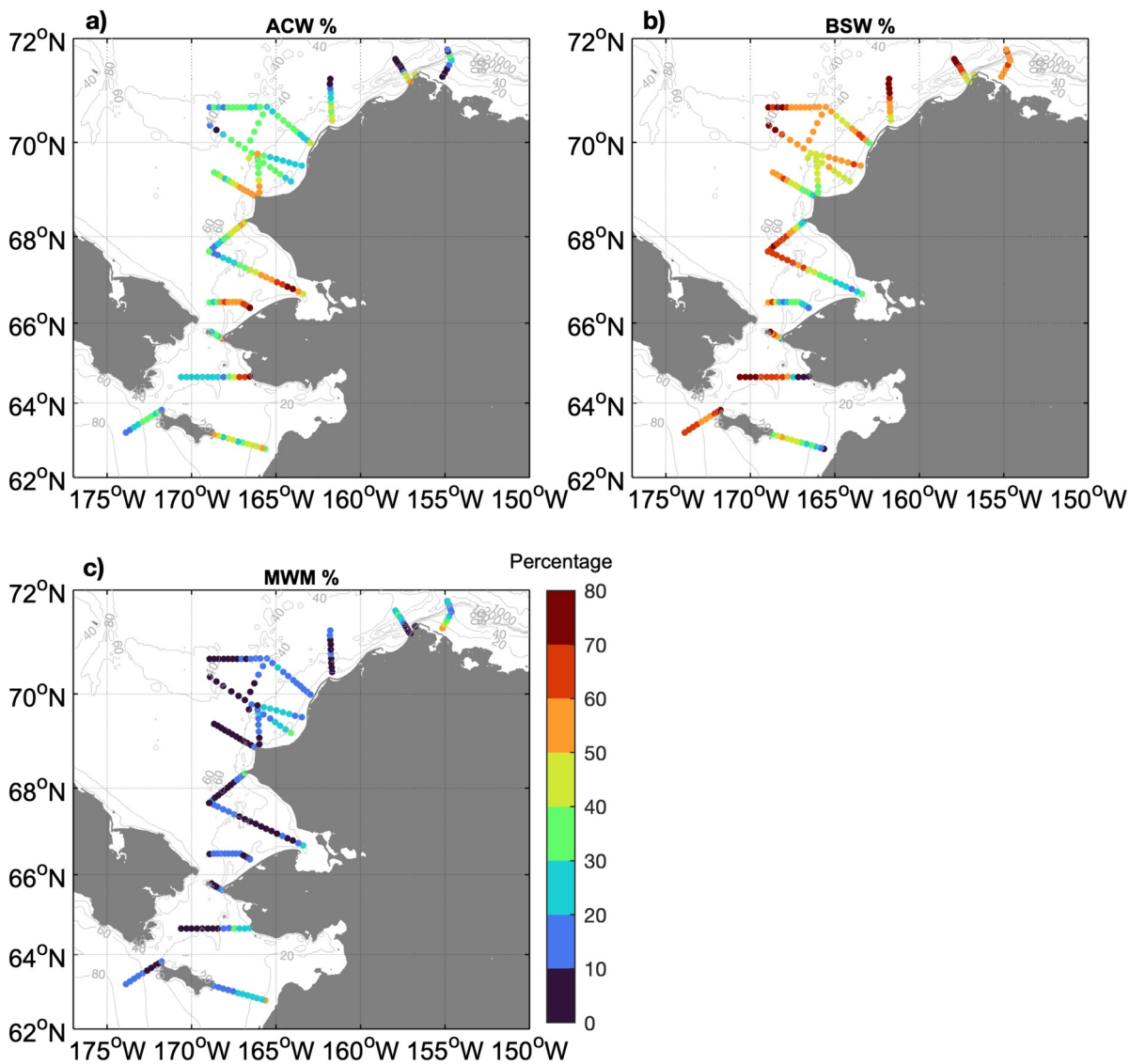

Figure 4. Lateral distributions of water mass percentages in the top 35 m of the water column during the northward portion of LEG 1 for (a) Alaskan Coastal Water, (b) Bering Summer Water, and (c) Melt water/Meteoric water. The bathymetry is from ETOPOv2.

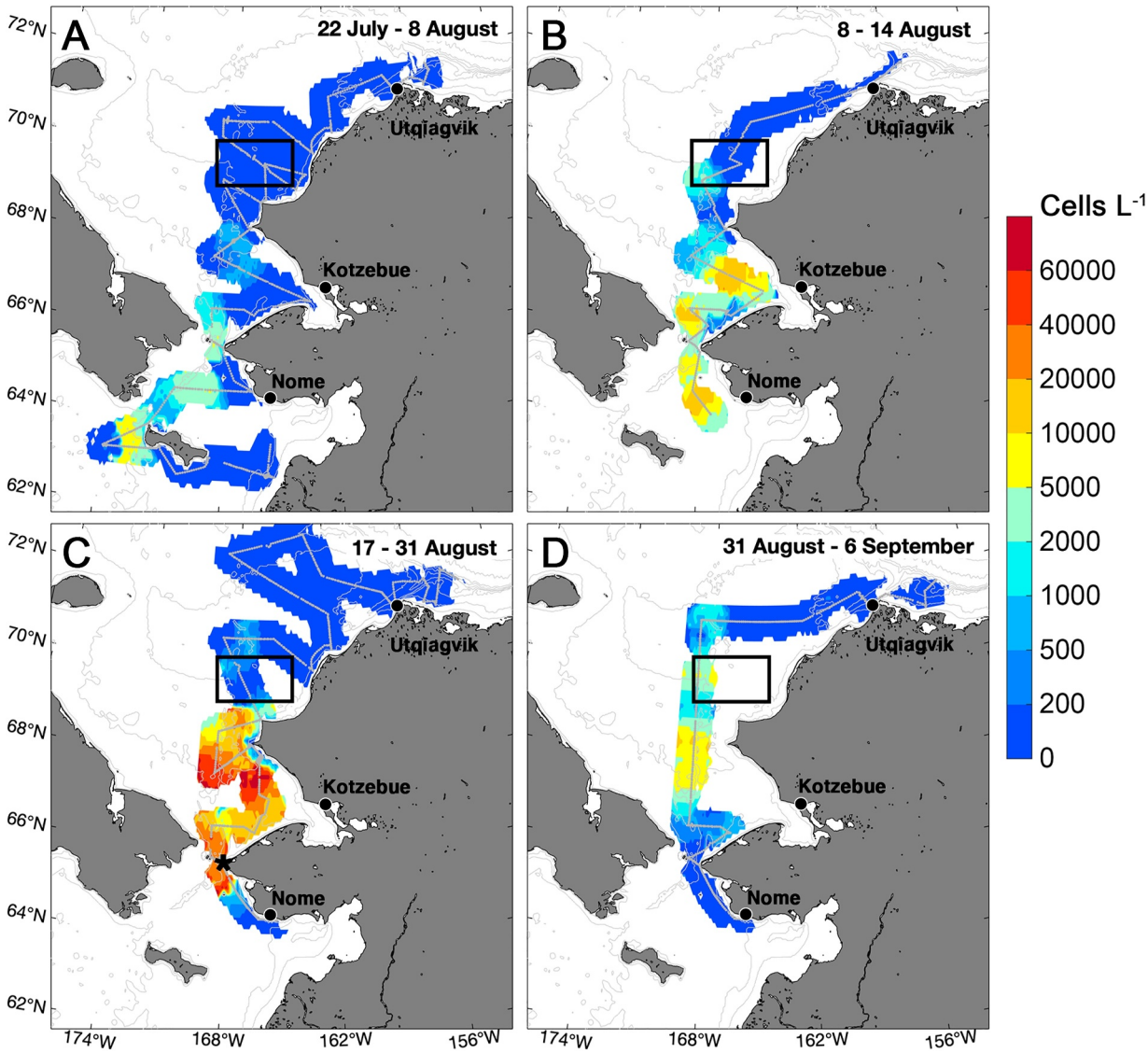

Figure 5. *Alexandrium catenella* concentrations measured by the IFCB during: (a) LEG 1 northward, (b) LEG 1 southward, (c) LEG 2 northward, and (d) LEG 2 southward, from Fachon et al. (2025). The black box indicates the Ledyard Bay region considered for the analysis of bottom temperature (see text). The bathymetry is from ETOPOv2.

discharge from Alaska. Farther to the north, there are some regions with enhanced MWM percentages that likely reflect sea ice melt.

3.2. Remote Bloom: Poleward Advection and Influence of the Wind

Using the IFCB data, Fachon et al. (2025) documented the general evolution of the HAB over the study period. To provide context for our analysis, we have reproduced Figure 1b from Fachon et al. (2025), showing the lateral distribution of *A. catenella* in near-surface waters for the northward and southward portions of each leg (Figure 5). The bloom was first detected in the southern part of the domain, with the largest concentrations west of St. Lawrence Island. In the subsequent month and a half, the bloom progressed northward through Bering Strait to roughly 71°N. It peaked in intensity within the study region in mid-August (Figure 5c).

An obvious question to ask is: where did the bloom emanate from? This cannot be answered using our in-situ data, since the measurements were restricted to US waters and did not extend southward of St. Lawrence Island. To address this, we carried out a backwards particle advection analysis (see Section 2.6) starting from the Kotzebue

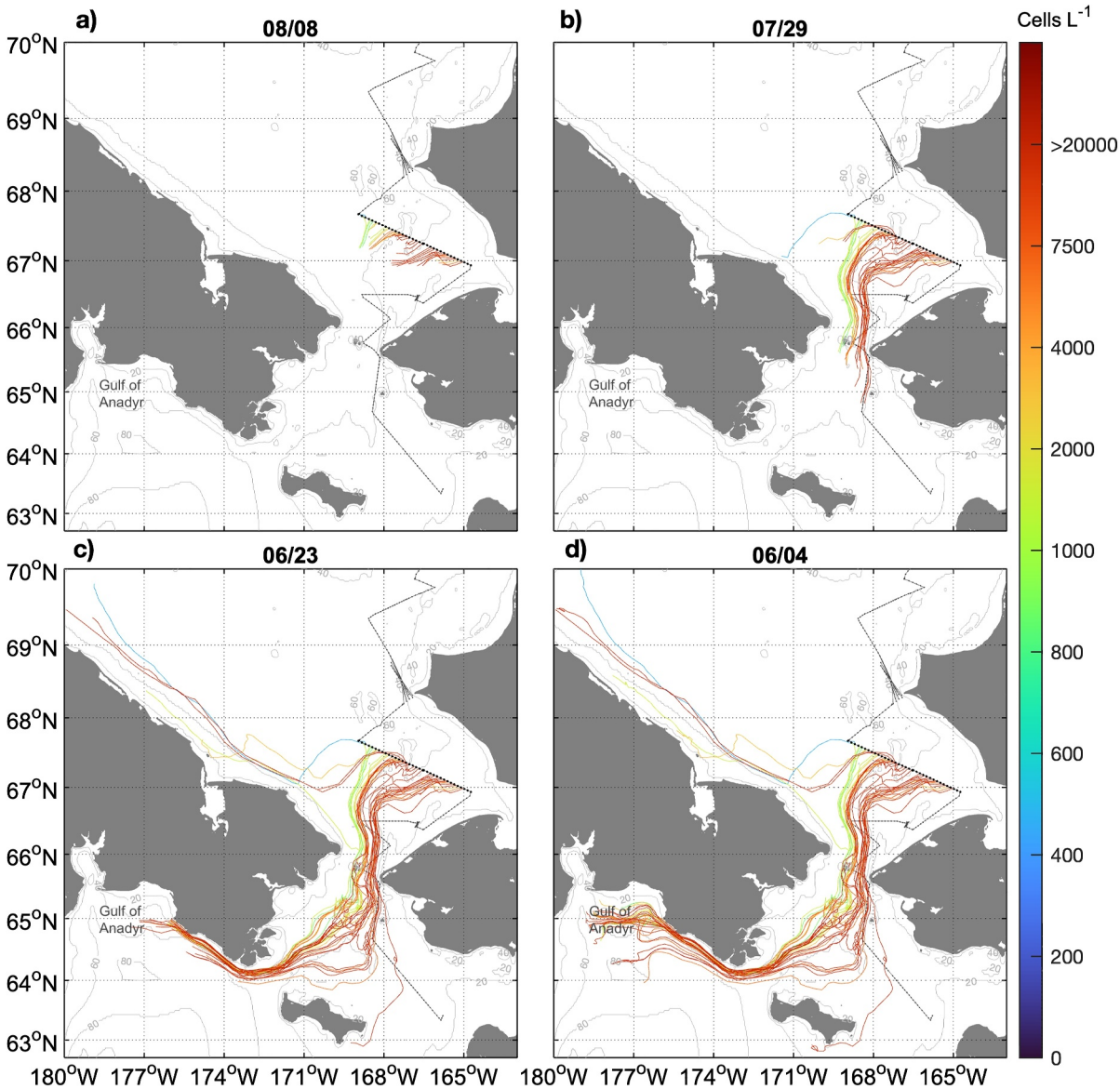

Figure 6. Trajectories resulting from the backwards particle advection experiment based on the GLORYS12v1 reanalysis velocities at 13 m depth. The end date is 12 August 2022, and the start date is: (a) August 8, (b) July 29, (c) June 23, and (d) June 4. The particle's end positions are indicated by the black dots, and the complete LEG 1 southward cruise track is indicated by the gray dotted line. The bathymetry is from ETOPOv2.

Sound section (KTZ, Figure 2a), occupied near the peak of the bloom. This region contained some of the highest concentrations of *A. catenella* measured during the entire field program. Particles were released at every GLORYS12v1 grid point along the line, color-coded by the nearest IFCB value. The results are shown in Figure 6.

The occupation of the KTZ section took place on August 12. Four days prior (Aug 8), the particles were south of the line flowing poleward as expected (Figure 6a). Ten days prior (July 29), the particles were passing through Bering Strait (Figure 6b), with the majority of the trajectories on the US side of the Strait. Those within the Russian channel had lower *A. catenella* concentrations by the time they reached KTZ. The trajectory map from 50 days prior (June 23) reveals that most of the trajectories passed through Anadyr Strait before making their way to the US side of Bering Strait (Figure 6c). A small number of trajectories extended east around St. Lawrence Island; these ended up on the inner-most part of Kotzebue Sound. Finally, 65 days prior to the occupation of the KTZ section (June 4), most of the particles were located within the Gulf of Anadyr.

A subsequent question based on the trajectory analysis is: did the bloom first originate from inside the Gulf of Anadyr? If so, germination would have had to occur in early June, as it took the water approximately 2 months to arrive in the Kotzebue Sound region. We did a DD analysis (see Section 2.7) for 2022 bottom temperatures in the northern Bering and Chukchi Seas and found that germination in the Gulf of Anadyr would have taken place mostly after the end of August due to the relatively cold bottom waters there earlier in the season (Figure S4 in Supporting Information S1). This is too late to be the source of the bloom observed during the *Norseman II* cruises. Furthermore, based on the GLORYS12v1 fields, advection from documented cyst accumulations farther south along the Russian coast of the Bering Sea (Orlova & Morozova, 2019) would take more than five months to arrive in the Bering Strait region.

Given that offshore bottom temperatures in the Gulf of Anadyr were not conducive to bloom initiation, there are at least three other possible scenarios to consider. One is that germination occurred within other cyst beds in the northern Bering Sea. However, given that the bloom was already quite dense when it was first detected west of St. Lawrence Island, it likely originated further afield, reinforcing the conclusion that it came from within the gulf. The second possibility is that germination could occur within the Gulf of Anadyr via resuspension of the resting cysts. Butman et al. (2014) show that storm-driven resuspension is likely to happen in waters shallower than 100 m, which is the case for the Gulf of Anadyr where bottom depths are shallower than 70 m. If there is an upwelling mechanism that can bring resuspended cysts to shallower and warmer waters, they could be subject to a more rapid accumulation of warming temperatures, as well as enhanced light availability and oxygenation, allowing them to germinate earlier and faster. However, it is important to note that while resuspended cysts can also be advected along transport pathways, previous studies (e.g., Aretxabaleta et al., 2014) have shown that they generally redeposit within a few kilometers of their source, so they are not likely to play a role in bloom initiation far from the cyst seedbed unless there are repeated resuspension events. The third and most likely scenario is that germination occurred in shallow embayments close to the coast within the Gulf of Anadyr, where bottom temperatures are warmer. The resulting vegetative cells could then be transported seaward, for example, by wind or tides. Ralston et al. (2015) demonstrated that this process can happen in embayments in the northeast US. Further study is required to investigate this scenario within the Gulf of Anadyr; however, the limited accessibility to Russian waters poses a significant challenge in this regard.

Considering the progression of the bloom (Figure 5), another question that we seek to answer is, why did the bloom reach its highest observed concentrations between 65 and 69°N during the second half of August? To address this, we computed the GR along each trajectory in Figure 6d (13 m depth), using the empirical formula described in Section 2.7. Results show that the *A. catenella* cells divide faster north of Bering Strait within Kotzebue Sound where it takes cells 4 days to double, while for the rest of the trajectories, cell division would take a week or longer (Figure 7). Indeed, the Kotzabue Sound part of the section is where the highest *A. catenella* concentrations were detected during the second half of August. These GR calculations also suggest that the initial population observed west of St. Lawrence Island was probably growing slowly, hence considerable time would have been needed during transport to achieve the relatively high cell concentrations (18,000 cells L^{-1}) observed there.

We note that the water emanating from Anadyr Strait measured on the northward portion of LEG1 was mainly BSW, or, more specifically, Anadyr Water (Figure 4). The high nutrient content of this water mass surely helped spur the HAB. However, based on temperature, the water that would support the fastest growth rates within Kotzebue Sound (Figure 7) was predominantly ACW (Figure 4; true for both the northward and southward portions of LEG1). The warm temperature of the ACW likely promoted the development of the bloom, so it is important to understand the transition of the water containing the bloom from BSW to ACW north of Bering Strait.

Typically the CC transports mainly BSW and passes to the west of Kotzebue Sound, while the ACC advects predominantly ACW and makes an incursion into the sound (Figure 1; Pickart et al., 2023). Using the *Norseman II* hydrographic and shipboard ADCP data, we distinguished the ACC and CC in the vicinity of Kotzebue Sound for the northward and southward portions of LEG 1. Figure 8 shows the near-surface flow vectors of the ACC in relation to the *A. catenella* concentrations for the two time periods. During the northward sampling, the bloom was not present in the ACC, but, during the southward sampling, the ACC was full of *A. catenella* cells which penetrated the inner part of the sound.

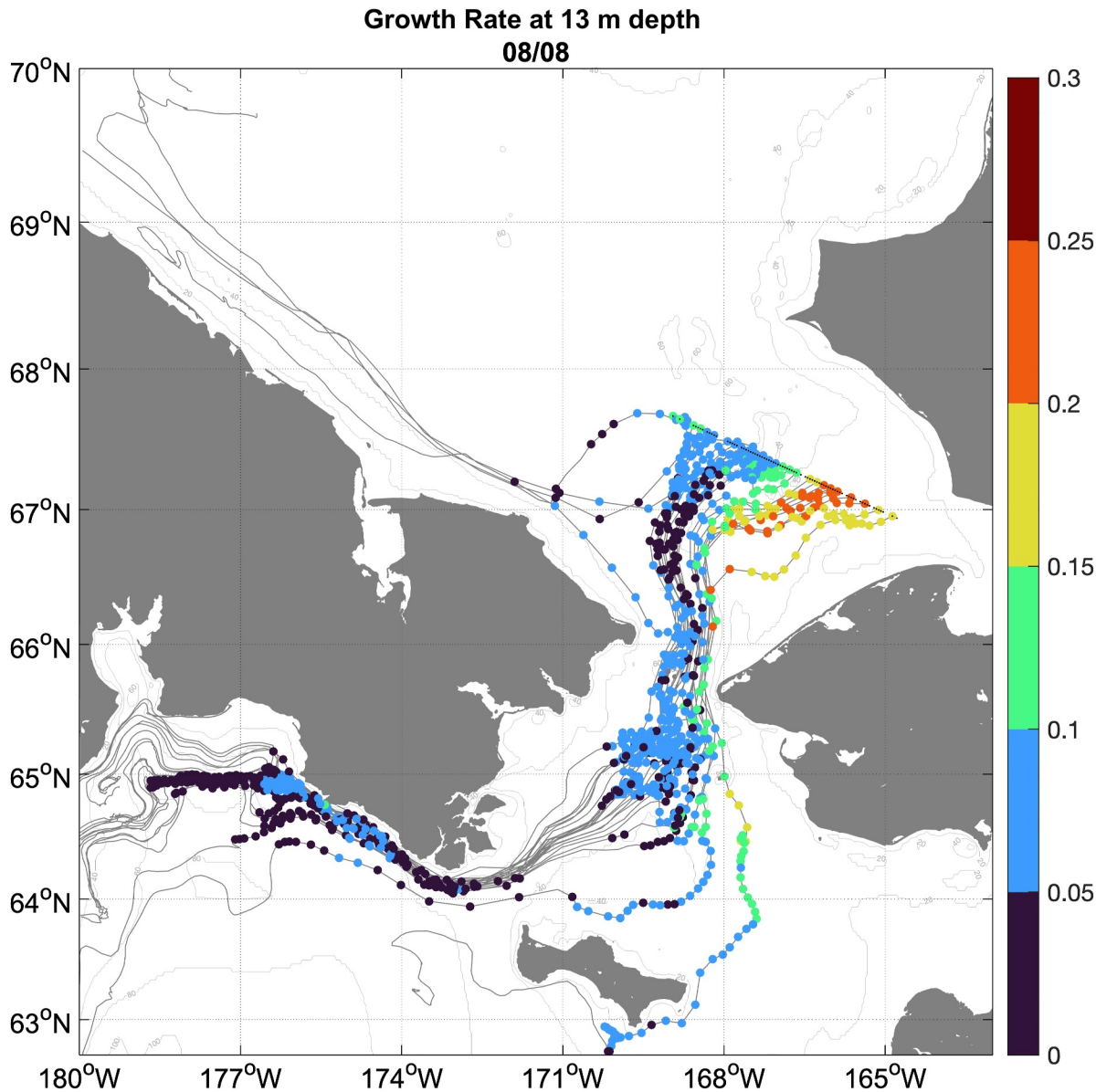

Figure 7. Growth rate (divisions per day) of *A. catenella* computed along each trajectory in Figure 6d, based on the GLORYS12v1 temperatures at 13 m depth and temperature-dependent growth rates of Chukchi Sea *A. catenella* isolates.

Coincident with the LEG 1 southward sampling, there was a strong southerly wind event with wind speeds exceeding 10 m s^{-1}. This would result in eastward Ekman transport into the sound which would advect the *A. catenella* cells shoreward while mixing the nutrient-rich BSW with the warm ACW. The ensuing geostrophic set-up would also cause stronger poleward flow of the ACC. As seen in Figure 8, the ACC is indeed stronger in the second period and the flow veered eastward. This interpretation is supported by data from the ChukSA shipboard ADCP climatology (2002–2023). We created two composite flow maps using the ChukSA data for the summer months (Jun–Sep): one for all wind conditions and one for just southerly wind conditions (exceeding 2 m s^{-1}) (Figures 9a and 9b). It is clear that the ACC is both strengthened and directed more to the east in the latter case. This is highlighted by the difference between the two composites which shows the anomalous eastward flow directly into Kotzebue sound during southerly wind conditions (Figure 9c).

These results highlight the importance of the anomalous wind in influencing the evolution of the HAB. Without this southerly wind event, most of the *A. catenella* cells would likely have remained within the CC and stayed

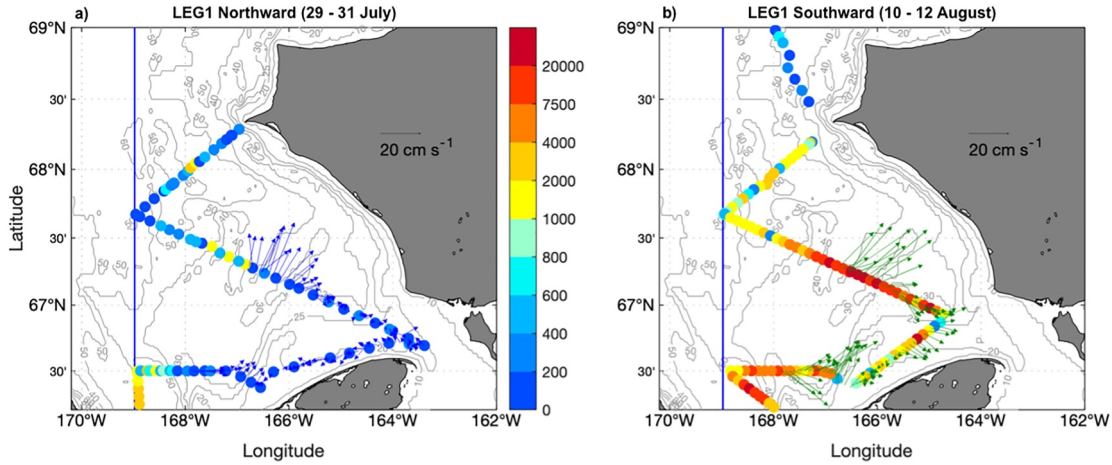

Figure 8. Near-surface flow of the Alaskan Coastal Current (vectors) and *A. catenella* concentrations (cells L^{-1}, colored dots) in the vicinity of Kotzebue Sound during the (a) northward and (b) southward sampling periods of LEG 1. The bathymetry is from ETOPOv2.

somewhat offshore of the Alaskan coast. We note that the ACW being transported in the ACC is much lower in nutrients than the BSW transported by the CC. Hence, while the 2022 bloom was first detected in the Bering Sea west of St. Lawrence Island within BSW, it is far less likely that a similar bloom would develop in the ACW east of St. Lawrence Island and be transported through Bering Strait in the ACC. Notably, in all of the Bering Strait crossings during our 2022 field program, the concentrations of *A. catenella* were considerably lower within the core of the ACC than in the BSW.

3.3. Local Bloom: Germination via Local Cyst Beds

Previous studies have documented an extensive cyst bed of *A. catenella* located in the Ledyard Bay region (Anderson, Fachon, et al., 2021). Cyst beds can be persistent features that are consistent in terms of location but which vary through time in terms of the total abundance of cysts (Brosnahan et al., 2017; Butman et al., 2014; Solow et al., 2014). The Ledyard Bay cyst bed was first noted by Natsuike et al. (2013), and our annual surveys since 2018 have documented a large and dense cyst bed every year, including on the 2022 cruise. These resting cysts could cause a local bloom if the environmental conditions are favorable; in particular, if bottom temperatures are warm enough to cause germination and if water column conditions, such as sufficient nutrients and warm temperatures, promote the subsequent growth of the vegetative cells. We now use the daily product from the GLORYS12v1 reanalysis in the Ledyard Bay region to better understand if/when local germination and growth was possible during summer 2022. Such a locally generated bloom would augment the remotely generated, advected HAB described in the previous section.

During the northward part of LEG 1, an extensive survey of the Ledyard Bay region was conducted (Figure 5a), during which *A. catenella* cells were present in the water column only in low densities (maximum concentrations ~70 cells L^{-1}). During the three other times that the *Norseman II* went through the region, only a single transect was occupied. Interestingly, higher concentrations were detected near the offshore part of the region all three times: to the southwest (LEG1 southward), northwest (LEG2 northward), and all along the west (LEG2 southward). In the final instance, cell concentrations close to 5,000 cells L^{-1} were measured. To help assess whether these signatures were the result of local bloom activity or an extension of the advected bloom, we compared the environmental conditions in 2022 to those in 2018 when there was a clear local bloom across the Ledyard Bay region with no evidence of an advected bloom emanating from the south (Anderson, Fachon, et al., 2021).

We first considered the potential for cyst germination by applying the DD model (Section 2.7). For each year from 1993 to 2023, we calculated the date when the 85 DD threshold was reached in the Ledyard Bay region (average of the box in Figure 5). This indicates that, on average, germination should occur around 12 August, with a standard deviation of 8 days (Figure 10). However, there is significant interannual variability in the expected timing of germination of the resting cysts, ranging over a month from as early as 23 July to as late as 27 August. For 2018, when the large local bloom was observed, the germination date was ~4 August, earlier than the mean

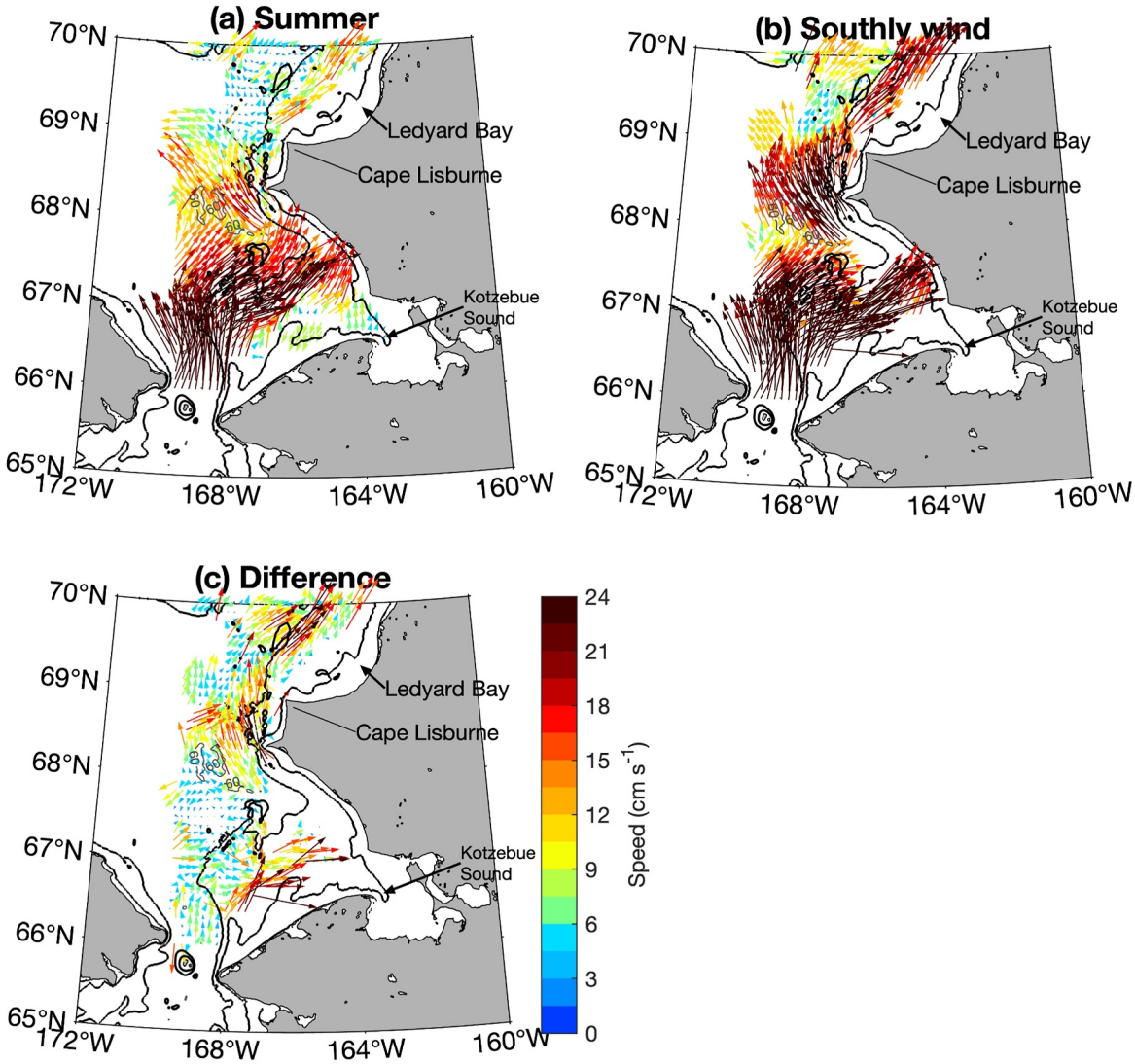

Figure 9. Composite flow maps in the vicinity of Kotzebue Sound using the ChukSA acoustic Doppler current profiler climatology. (a) Summertime mean (Jun–Sep) for all wind conditions. (b) Summertime mean for southerly winds exceeding 2 m s^{-1}. (c) The difference between the two composites (southerly wind case minus all wind case). The vectors are color coded according to flow speed (cm s^{-1}). The bathymetry is from ETOPOv2.

date. By comparison, the germination date for 2022 was ∼7 August, close to that for 2018. This implies that cumulative bottom temperatures in the Ledyard Bay region were generally favorable for germination in 2022.

Next, to assess whether the water column temperatures were conducive for subsequent vegetative growth, we analyzed the GR of cells based on the temperatures at 13 m depth in the Ledyard Bay region (Figure 11). We note that this includes part of the region with high concentrations of vegetative cells (above 500 cells L^{-1}) reported by Anderson, Fachon, et al. (2021) for a composite of 2018 and 2019. Positive growth rates (above 0 divisions day^{-1}) were possible between June 18 and November 13 in 2018, while in 2022 this period was 37 days shorter, from July 8 to October 27. In 2022, when the 85 DD germination threshold was reached on August 7, average surface temperatures of roughly 6°C would support a GR of ∼0.14 divisions per day, or ∼7 days for a single population doubling. By contrast, when the region reached the 85 DD threshold on 4 August 2018, average surface temperatures of roughly 8°C would support a GR of ∼0.23 divisions per day, or ∼4 days for a single population doubling. Taken together, this implies that, once germination occurred, the cells found more suitable temperatures to divide quickly in 2018 than in 2022, likely leading to a stronger and earlier bloom in 2018.

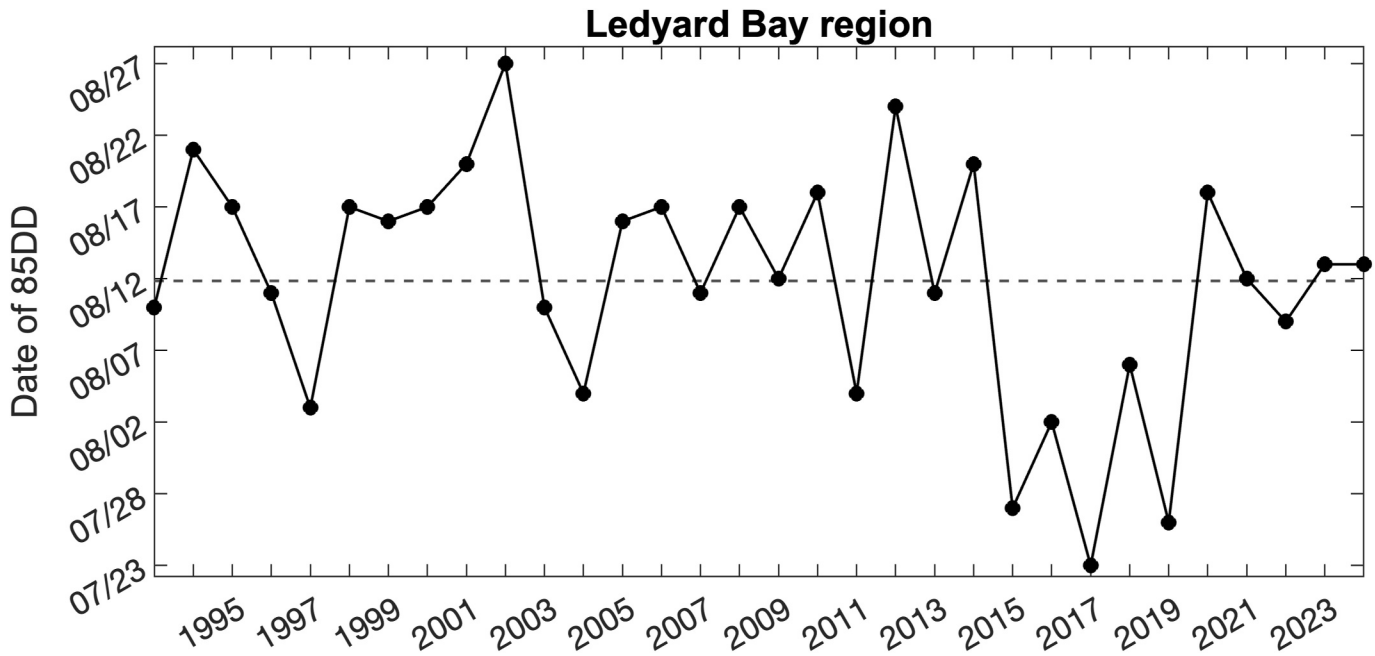

Figure 10. Date of the year when the 85 degree-day (85DD) threshold is reached in the Ledyard Bay region using the GLORS12v1 bottom temperatures (see Figure 5 for the location of the Ledyard Bay box). The dashed line is the mean.

In light of these results, one is tempted to conclude that there was weaker local bloom activity in the Ledyard Bay region during the 2022 *Norseman II* study period. However, during both the northward and southward portions of LEG2 we did not collect water samples in the eastern half of the Ledyard Bay region where the cyst bed is most dense (Anderson, Fachon, et al., 2021). It should be noted as well that when the vegetative cell signal first appeared in this region (during the southward portion of LEG1 and northward portion of LEG2, Figures 5b and 5c) it was isolated from the signal to the south, suggesting that it may not have been connected to the remotely generated bloom. As such, while there was a massive remotely generated bloom in summer 2022, we don't have

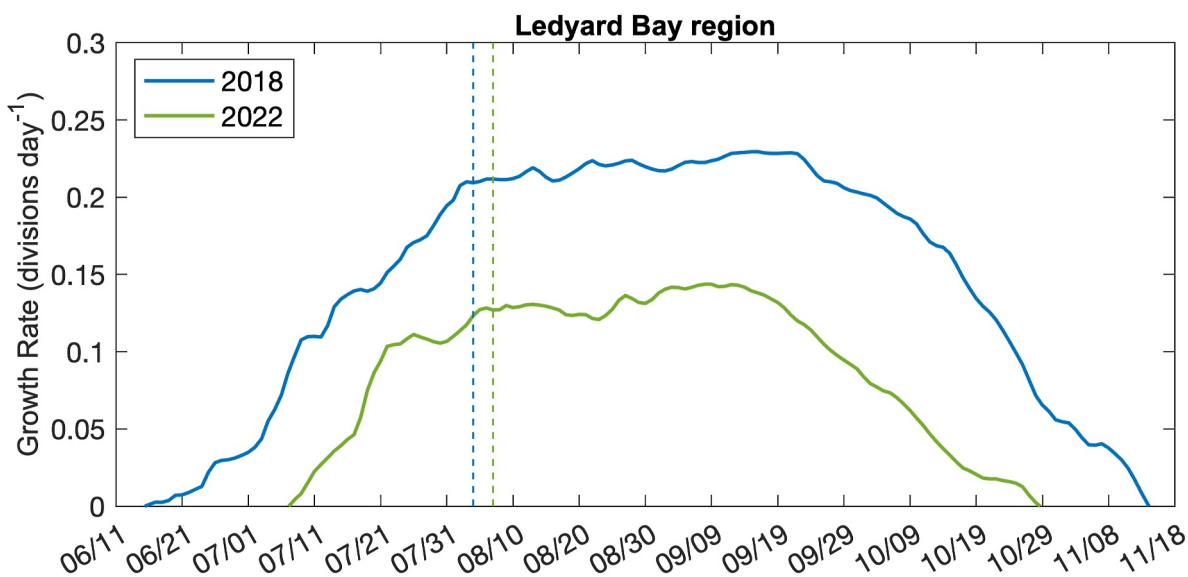

Figure 11. Growth rate of the *A. catenella* cells based on near-surface (13 m) temperatures for the Ledyard Bay box shown in Figure 5, for 2018 (blue) and 2022 (green). The dashed lines show the day of each year when bottom temperatures in the region reach the 85DD threshold.

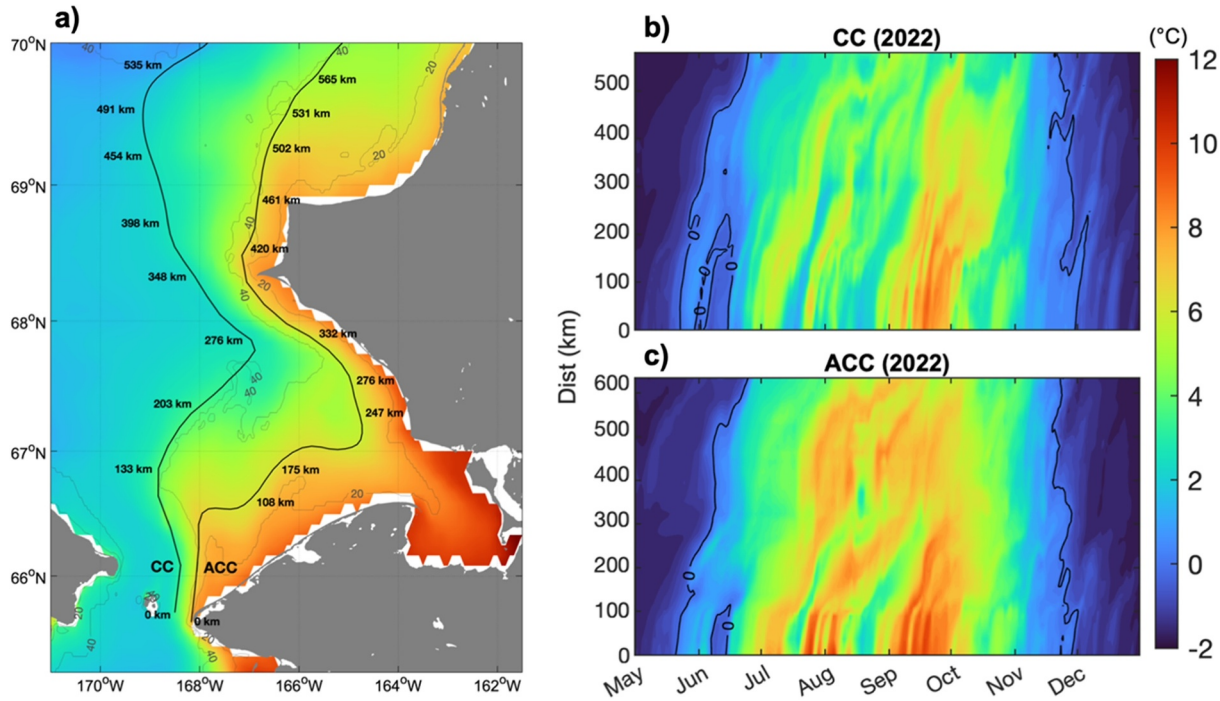

Figure 12. (a) The ACC and CC pathways (solid black lines) used to construct the bottom temperature Hovmöller plots described in the text, overlaid on the GLORYS12v1 summer mean bottom temperature for 2022 (color). The distances along the pathways are indicated. (b) Hovmöller of bottom temperature along the CC pathway from May through December 2022. (c) Same as (b) except for the ACC. The black contours in panels (b) and (c) denote the 0°C isotherm.

enough information to determine definitively to what extent the Ledyard Bay cyst bed might have contributed to the observed HAB signal at these higher latitudes.

Due to the persistent yearly presence of the Ledyard Bay cyst bed, its extraordinary size and abundance, and the pronounced inter-annual variability in DD in that region (Figure 10), it is important to determine what drives the year-to-year changes in summer bottom water temperatures there. To investigate this, we first seek to identify the propagation of heat from Bering Strait toward Ledyard Bay by constructing Hovmöller plots of bottom temperature using the GLORYS12v1 fields along two different pathways: one corresponding to the ACC and the other corresponding to the CC (Figure 12a). The selection of these pathways is based on the trajectories occupied by particles in a forward advection calculation starting in Bering Strait, based on the mean 2022 summer velocities. The two trajectories are roughly coincident with bottom isotherms in the mean 2022 summer temperature field. Both Hovmöller plots clearly show the poleward propagation of heat along the Chukchi shelf (Figures 12b and 12c). The striations in temperature through the season are due to occasional periods when colder water is flowing through Bering Strait, for example, following a wind-driven upwelling event. Not surprisingly, more heat is transported along the ACC.

Next, we compared the Hovmöller plots along the ACC pathway for 2018 and 2022 (Figure 13). Note that the warming above 0°C started approximately 15 days earlier in 2018 (early May vs. late May) and that the summer bottom water temperatures were higher that year, with differences of roughly 3°C. As seen in Figure 13, the pattern of propagation from Bering Strait to the Ledyard Bay region is the same in both years: faster velocities between Bering Strait and 66.6°N and also between 67.5°N and 68.8°N, with slower velocities for the remainder of the pathway. This is true of all years due to the variation in topography along the ACC (e.g., Pisareva et al., 2015). While there is significant interannual variability in the propagation speed along these four segments, the time of propagation from Bering Strait to the Ledyard Bay region was similar for both 2018 and 2022, approximately 45 days. Hence, the slightly earlier (3–4 days) germination date in 2018 could be due to the warmer water carried by the ACC that year.

Knowing that the poleward propagation of heat through Bering Strait modulates the bottom temperatures in the Ledyard Bay region on interannual timescales, we then analyzed the heat transport across Bering Strait based on

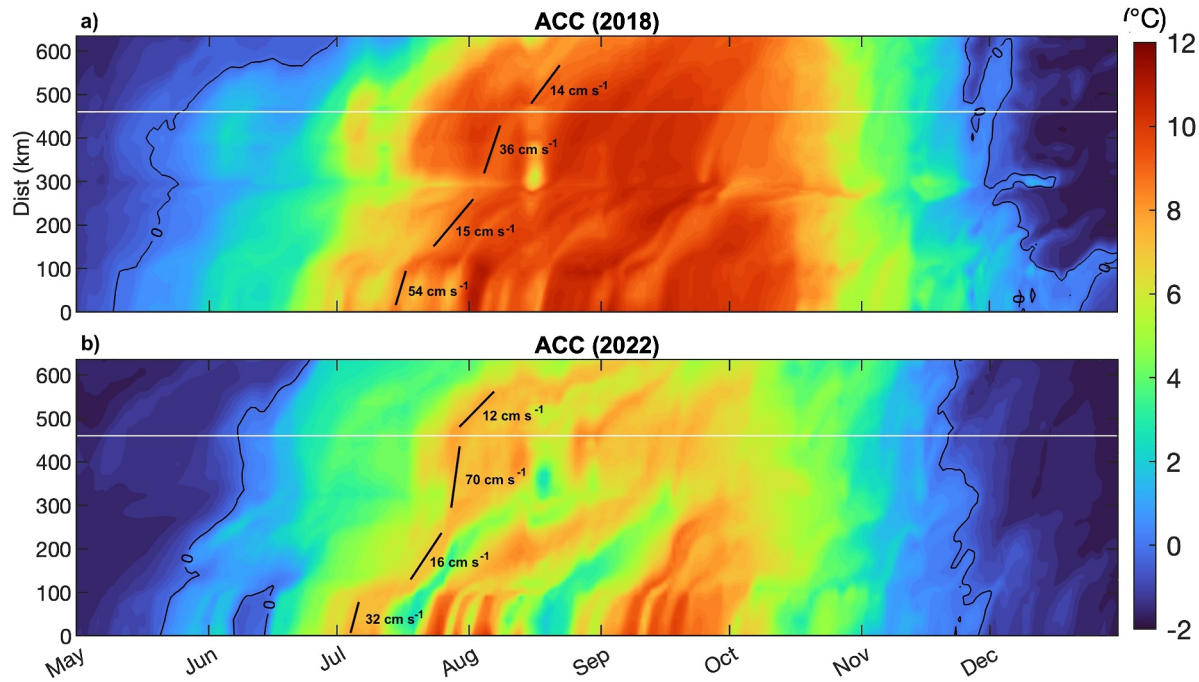

Figure 13. Hovmöller plot of bottom temperature along the Alaskan Coastal Current pathway from May through December for (a) 2018 and (b) 2022. The four segments of the pathway are marked by the black lines, including estimates of the velocity along each segment. The black contours in panels (a) and (b) denote the 0°C isotherm. The horizontal white line indicates where the Ledyard Bay region begins.

the GLORYS12v1 reanalysis temperature and velocity fields (Section 2.8). We note that the section extends across the Russian side of the strait as well. The variability is similar on both sides, but the magnitude of the transport is greater (by 0.5 10^{13} W) on the US side.

We computed the monthly averaged near-bottom heat transport for the summer months and constructed yearly timeseries for each of the months. These were then compared to the germination timeseries of Figure 10, by estimating the Pearson correlation coefficient for a 95% confidence level (Wilks, 2011). Correlations for both May and June are ~0.75 and statistically significant, implying that a larger Bering Strait near-bottom heat flux during those months is associated with an earlier initiation of the germination (Figure S5 in Supporting Information S1). The correlations would likely be even higher were it not for the effect of local heating on the Chukchi shelf when there is open water (see, for example, Pickart et al. (2023)) and the fact that the propagation time varies each year.

Lastly, it is important to note that the Bering Strait heat flux in the shallower part of the water column will influence the peak timing and intensity of a local HAB occurring in the Ledyard Bay region. Recall that, based on the temperature-dependent GR calculation for the near-surface water, *A. catenella* vegetative cells had a higher GR in the Ledyard Bay region in 2018 than in 2022. Moreover, faster division occurred earlier in the year in 2018 than in 2022, and lasted longer. The connection to Bering Strait is evident in the mean summer vertical sections for temperature and velocity across the strait for 2018 versus 2022 (Figure 14). The near-bottom velocity is the same in both years, but the near-bottom temperature is slightly warmer in 2018, consistent with the above results regarding germination. At the same time, the upper layer is significantly warmer and the upper layer flow is stronger in 2018 than in 2022, consistent with the peak bloom timing discussed above. This highlights the importance of the Bering Strait heat flux in influencing both the timing of local germination of the *A. catenella* cyst bed in the Ledyard Bay region as well as the subsequent growth rates of the vegetative cells there.

4. Discussion

The IFCB and shipboard velocity data presented in Fachon et al. (2025) suggest there were two possible pathways in the northern Bering Sea associated with the high *A. catenella* concentrations: one that flows through the Anadyr Strait and another between St. Lawrence Island and the Alaskan Coast (Anderson et al., 2022). Our backward

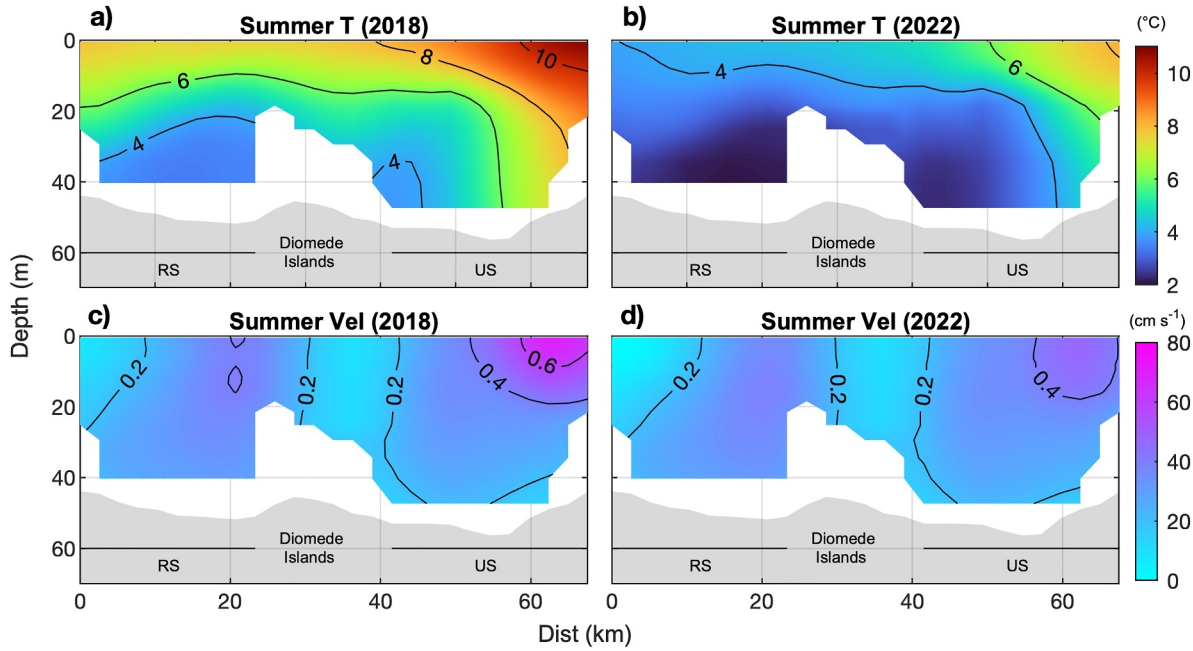

Figure 14. (a) Summer mean vertical section of temperature across Bering Strait in 2018. (b) Same as (a) except for 2022. (c) Summer mean vertical section of velocity across Bering Strait in 2018; positive values are poleward. (d) Same as (c) except for 2022. RS stands for Russia Side, US stands for United States side.

trajectory results confirm that the water we observed transporting the 2022 HAB emanated from the vicinity of the Gulf of Anadyr and mostly passed through Anadyr Strait (84% of the trajectories), rather than south and east of St. Lawrence Island (4% of the trajectories), before transiting through the US side of Bering Strait into the Chukchi Sea. We note that very few of the high concentrations of *A. catenella* cells detected on the KTZ line could have emanated from the Siberian Coastal Current (12% of the trajectories, Figures 6c and 6d). As little is known about the presence of *A. catenella* cells or cysts along the Siberian coast, it is not possible to comment on the likelihood of that region being a source of *A. catenella* cells in this bloom event, though the predominant bloom progression was clearly poleward through Bering Strait. It is important to keep in mind that the pathways discussed here are associated with this specific bloom and where we observed it, and do not imply that *A. catenella* cells were not present on the Russian side of Bering Strait. Furthermore, the pathway to the east of St. Lawrence Island could play a more important role in other years.

While the warm temperatures of ACW can promote *A. catenella* growth, this effect may be tempered by the relatively low nutrient content of this water mass, which can limit phytoplankton growth. This suggests that the communities along the coast of the Chukchi Sea might be somewhat shielded from the highly toxic effects of such HABs originating from the Bering Sea (although many of their food resources such as walrus, seals, and seabirds forage offshore). Indeed, the water measured in the ACC flowing through Bering Strait during our study had markedly lower *A. catenella* concentrations than that sampled on the western side of the US strait in the BSW. However, southerly wind events such as the one occurring in August 2022 during the southward portion of LEG2 would counteract this by diverting blooms further east toward the coast and promoting mixing between BSW and ACW, creating growth conditions that are conducive in respect to both temperature and nutrients. There is evidence that such wind events in the northern Bering Sea have been increasing (Stabeno & Bell, 2019) and that this trend will continue in the coming decades (Hermann et al., 2019). Tachibana et al. (2019) suggest that low ice anomalies in the Chukchi Sea lead to southerly wind anomalies there. In light of the decreasing regional ice cover (Frey et al., 2023), this would imply a more common occurrence of such winds. Based on the ERA5 atmospheric reanalysis data, the occurrence of southerly winds during the months of July and August in the Chukchi Sea shows no significant long-term trend. However, during July, 11 of the 30 years considered had more than 50% of the days during the month with southerly wind conditions, including five of the last seven years (2017, 2018, 2019, 2021, and 2023).

It is now evident that massive HABs in the Chukchi Sea can originate remotely in the northern Bering Sea and be advected through Bering Strait, such as the 2022 event analyzed here, or be primarily formed locally due to germination of the large cyst bed in the Ledyard Bay region, such as the 2018 event reported by Anderson, Fachon, et al. (2021). What remains unclear is the extent to which both scenarios can happen in the same year and how frequently this might take place. Our results indicate, however, that summer Bering Strait heat transport impacts both the germination of cysts and cell growth in the Ledyard Bay region as well as any subsequent water column bloom there. Further work is needed to identify analogous environmental indicators of advected blooms from the Bering Sea, which will be an important step forward toward predicting regional HABs. It is also of high interest to use population genetics in future studies in order to discriminate different *A. catenella* populations in the region. Moreover, as this species has unique toxin profiles that can be geographically distinct, the relationships between different populations should be pursued using toxin profiling, as in Natsuike, Oikawa, et al. (2017). Further studies of this type are currently underway.

5. Summary

Using an extensive set of in-situ measurements collected on two back-to-back cruises in summer 2022, in conjunction with the GLORYS12v1 reanalysis product, we investigated the physical drivers of a massive *Alexandrium catenella* HAB detected in the northern Bering and Chukchi Seas, as well as the role of interannual temperature variability in facilitating bloom activity on the Chukchi Shelf. The measured concentrations of the toxic dinoflagellate *Alexandrium catenella* were the highest ever recorded in the region, with values exceeding 170,000 cells L^{-1} (Fachon et al., 2025). This expansive bloom provided a unique opportunity to document the hydrographic conditions which accompanied the bloom development. Notably, this species produces PSTs that are among the most globally widespread of all HAB poisoning syndrome toxins (Anderson et al., 2012; Anderson, Fensin, et al., 2021).

The bloom was first detected at the end of July west of St. Lawrence Island, embedded in BSW. In the following weeks, the cells were advected poleward. Using a backward trajectory analysis, we demonstrated that the main pathway of the observed vegetative cells was from within the Gulf of Anadyr, through Anadyr Strait, and through the US side of Bering Strait. Warm surface temperatures north of Bering Strait enhanced the growth of vegetative cells along the trajectories, and a southerly wind event mixed the high-nutrient Bering Summer Waters with warm Alaskan Coastal Waters, further promoting growth near the US coast. While the bulk of the 2022 Chukchi Sea HAB emanated from the northwestern Bering Sea and was advected northward, it is less clear if local germination and growth also occurred from the large cyst bed in the Ledyard Bay region. According to a degree-day analysis of bottom temperatures, germination should have occurred in early August, similar to 2018 when a large local HAB was observed near Ledyard Bay. However, a GR analysis based on the near-surface temperatures implies that the locally germinated cells in 2022 would have had lower division rates than in 2018.

With regard to local germination, it was demonstrated that the interannual variability of the near-bottom heat transport through Bering Strait impacts the bottom temperatures over the cyst bed in the Ledyard Bay region—which in turn dictates when germination can be initiated each summer. Furthermore, the heat transport in the upper part of the water column in Bering Strait influences the subsequent growth of the vegetative cells emanating from the cyst bed. Going forward, it is of high interest to better understand the interplay between such locally formed blooms and the remotely formed blooms stemming from the Bering Sea.

Data Availability Statement

The CTD data from the R/V *Norseman II* cruises are available at https://arcticdata.io/catalog/view/doi%3A10.18739%2FA2B853K56, and the shipboard ADCP data are available at https://scienceweb.whoi.edu/seasoar/chukchi_sadcp/. The underway temperature/salinity and bloom abundance data used in the study reside at https://arcticdata.io/catalog/view/doi%3A10.18739%2FA2804XM7S.

Acknowledgments
The authors are indebted to the captain and crew of the R/V *Norseman II* for their dedication and hard work in making the two back-to-back cruises in summer 2022 safe and successful. Support Vessels of Alaska installed a new underway flow through system on the ship which was critical for our measurements; we are grateful to Scott Hameister for making this happen. Marshall Swartz went to great effort to prepare and test the CTD system used for the fieldwork, and Leah McRaven did the final quality control and calibration of the CTD data and underway physical data. A group of dedicated watchstanders enabled the collection of such a large data set, often under challenging conditions. This work was funded under National Science Foundation grant OPP-1823002. Analysis support was provided by the Arctic Research Program of the National Oceanic and Atmospheric Administration, grant NA19OAR4320074 (through the Cooperative Institute for the North Atlantic Region). D.A. and his laboratory personnel were supported by NOAA's Arctic Research program (through the Cooperative Institute for the North Atlantic Region (NA14OAR4320158 and NA19OAR4320074)); NOAA's Centers for Coastal and Ocean Science Compatitive Research Program under award NA20NOS4780195; The Woods Hole Center for Oceans and Human Health (National Science Foundation grant OCE-1840381 and National Institutes of Health grant NIEHS-1P01-ES028938-01). E.F. was supported by the National Science Foundation Graduate Research Fellowship Grants 2141064 and a North Pacific Research Board Graduate Student Research Award. P.L. was supported by National Natural Science Foundation of China (42306251) and the Shanghai Pujiang Program (22PJ1406400). This is ECOHAB Contribution number ECO1117.

References

Anderson, D. (2014). HABs in a changing world: A perspective on harmful algal blooms, their impacts, and research and management in a dynamic era of climactic and environmental change. In *Harmful Algae 2012: Proceedings of the 15th International Conference on Harmful Algae : October 29 - November 2, 2012, CECO, Changwon, Gyeongnam, Korea/Editors, Hak Gyoon Kim, Beatriz Reguera, Gustaaf M. Hallegraeff, Chang Kyu Lee, M., 2012* (pp. 3–17).

Anderson, D. M., Alpermann, T. J., Cembella, A. D., Collos, Y., Masseret, E., & Montresor, M. (2012). The globally distributed genus *Alexandrium*: Multifaceted roles in marine ecosystems and impacts on human health. *Harmful Algae*, *14*, 10–35. https://doi.org/10.1016/j.hal.2011.10.012

Anderson, D. M., Fachon, E., Hubbard, K., Lefebvre, K. A., Lin, P., Pickart, R., et al. (2022). Harmful algal blooms in the alaskan arctic. *Oceanography*, *35*(3/4), 130–139.

Anderson, D. M., Fachon, E., Pickart, R. S., Lin, P., Fischer, A. D., Richlen, M. L., et al. (2021). Evidence for massive and recurrent toxic blooms of Alexandrium catenella in the Alaskan Arctic. *Proceedings of the National Academy of Sciences of the United States of America*, *118*(41), e2107387118. https://doi.org/10.1073/pnas.2107387118

Anderson, D. M., Fensin, E., Gobler, C. J., Hoeglund, A. E., Hubbard, K. A., Kulis, D. M., et al. (2021). Marine harmful algal blooms (HABs) in the United States: History, current status and future trends. *Harmful Algae*, *102*, 101975. https://doi.org/10.1016/j.hal.2021.101975

Anderson, D. M., Kulis, D. M., Keafer, B. A., Gribble, K. E., Marin, R., & Scholin, C. A. (2005). Identification and enumeration of *Alexandrium* spp. from the Gulf of Maine using molecular probes. *Deep Sea Research Part II: Topical Studies in Oceanography*, *52*(19), 2467–2490. https://doi.org/10.1016/j.dsr2.2005.06.015

Aretxabaleta, A. L., Butman, B., Signell, R. P., Dalyander, P. S., Sherwood, C. R., Sheremet, V. A., & McGillicuddy, D. J. (2014). Near-bottom circulation and dispersion of sediment containing *Alexandrium fundyense* cysts in the Gulf of Maine during 2010–2011. *Deep Sea Research Part II: Topical Studies in Oceanography*, *103*, 96–111. https://doi.org/10.1016/j.dsr2.2013.11.003

Arrigo, K. R., Mills, M. M., van Dijken, G. L., Lowry, K. E., Pickart, R. S., & Schlitzer, R. (2017). Late spring nitrate distributions beneath the ice-covered northeastern Chukchi shelf. *Journal of Geophysical Research: Biogeosciences*, *122*(9), 2409–2417. https://doi.org/10.1002/2017JG003881

Arrigo, K. R., Perovich, D. K., Pickart, R. S., Brown, Z. W., van Dijken, G. L., Lowry, K. E., et al. (2012). Massive phytoplankton blooms under Arctic sea ice. *Science*, *336*(6087), 1408. https://doi.org/10.1126/science.1215065

Arrigo, K. R., Perovich, D. K., Pickart, R. S., Brown, Z. W., Van Dijken, G. L., Lowry, K. E., et al. (2014). Phytoplankton blooms beneath the sea ice in the Chukchi sea. *Deep Sea Research Part II: Topical Studies in Oceanography*, *105*, 1–16. https://doi.org/10.1016/j.dsr2.2014.03.018

Bravo, I., Vila, M., Masó, M., Figueroa, R. I., & Ramilo, I. (2008). *Alexandrium catenella* and *Alexandrium minutum* blooms in the Mediterranean Sea: Toward the identification of ecological niches. *Harmful Algae*, *7*(4), 515–522. https://doi.org/10.1016/j.hal.2007.11.005

Brosnahan, M. L., Ralston, D. K., Fischer, A. D., Solow, A. R., & Anderson, D. M. (2017). Bloom termination of the toxic dinoflagellate Alexandrium catenella: Vertical migration behavior, sediment infiltration, and benthic cyst yield. *Limnology & Oceanography*, *62*(6), 2829–2849. https://doi.org/10.1002/lno.10664

Brosnahan, M. L., Velo-Suárez, L., Ralston, D. K., Fox, S. E., Sehein, T. R., Shalapyonok, A., et al. (2015). Rapid growth and concerted sexual transitions by a bloom of the harmful dinoflagellate Alexandrium fundyense (Dinophyceae). *Limnology & Oceanography*, *60*(6), 2059–2078. https://doi.org/10.1002/lno.10155

Butman, B., Aretxabaleta, A. L., Dickhudt, P. J., Dalyander, P. S., Sherwood, C. R., Anderson, D. M., et al. (2014). Investigating the importance of sediment resuspension in *Alexandrium fundyense* cyst population dynamics in the Gulf of Maine. *Deep Sea Research Part II: Topical Studies in Oceanography*, *103*, 79–95. https://doi.org/10.1016/j.dsr2.2013.10.011

Carvalho, K. S., Smith, T. E., & Wang, S. (2021). Bering Sea marine heatwaves: Patterns, trends and connections with the Arctic. *Journal of Hydrology*, *600*, 126462. https://doi.org/10.1016/j.jhydrol.2021.126462

Coachman, L. K., & Aagaard, K. (1988). Transports through Bering Strait: Annual and interannual variability. *Journal of Geophysical Research*, *93*(C12), 15535–15539. https://doi.org/10.1029/JC093iC12p15535

Condie, S. A., Oliver, E. C. J., & Hallegraeff, G. M. (2019). Environmental drivers of unprecedented *Alexandrium catenella* dinoflagellate blooms off eastern Tasmania, 2012–2018. *Harmful Algae*, *87*, 101628. https://doi.org/10.1016/j.hal.2019.101628

Danielson, S. L., Ahkinga, O., Ashjian, C., Basyuk, E., Cooper, L. W., Eisner, L., et al. (2020). Manifestation and consequences of warming and altered heat fluxes over the Bering and Chukchi Sea continental shelves. *Deep Sea Research Part II: Topical Studies in Oceanography*, *177*, 104781. https://doi.org/10.1016/j.dsr2.2020.104781

Danielson, S. L., Grebmeier, J. M., Iken, K., Berchok, C., Britt, L., Dunton, K. H., et al. (2022). Monitoring Alaskan Arctic shelf ecosystems through collaborative observation networks. *Oceanography*, *35*(3/4), 198–209. https://doi.org/10.5670/oceanog.2022.119

Danielson, S. L., Weingartner, T. J., Hedstrom, K. S., Aagaard, K., Woodgate, R., Curchitser, E., & Stabeno, P. J. (2014). Coupled wind-forced controls of the Bering–Chukchi shelf circulation and the Bering Strait throughflow: Ekman transport, continental shelf waves, and variations of the Pacific–Arctic sea surface height gradient. *Progress in Oceanography*, *125*, 40–61. https://doi.org/10.1016/j.pocean.2014.04.006

Fachon, E., Pickart, R. S., Sheffield, G., Pate, E., Pathare, M., Brosnahan, M. L., et al. (2025). Tracking a large-scale and highly toxic Arctic algal bloom: Rapid detection and risk communication. *Limnology and Oceanography Letters*, *10*(1), 62–72. https://doi.org/10.1002/lol2.10421

Fischer, A. D., Brosnahan, M. L., & Anderson, D. M. (2018). Quantitative response of *Alexandrium catenella* cyst dormancy to cold exposure. *Protist*, *169*(5), 645–661. https://doi.org/10.1016/j.protis.2018.06.001

Frey, K. E., Comiso, J. C., Stock, L. V., Young, L. N. C., Cooper, L. W., & Grebmeier, J. M. (2023). A comprehensive satellite-based assessment across the Pacific Arctic Distributed Biological Observatory shows widespread late-season sea surface warming and sea ice declines with significant influences on primary productivity. *PLoS One*, *18*(7), e0287960. https://doi.org/10.1371/journal.pone.0287960

Gong, D., & Pickart, R. S. (2015). Summertime circulation in the eastern Chukchi Sea. *Deep Sea Research Part II: Topical Studies in Oceanography*, *118*, 18–31. https://doi.org/10.1016/j.dsr2.2015.02.006

Grebmeier, J. M. (2012). Shifting patterns of life in the Pacific Arctic and sub-Arctic seas. *Annual Review of Marine Science*, *4*(1), 63–78. https://doi.org/10.1146/annurev-marine-120710-100926

Grebmeier, J. M., Bluhm, B. A., Cooper, L. W., Danielson, S. L., Arrigo, K. R., Blanchard, A. L., et al. (2015). Ecosystem characteristics and processes facilitating persistent macrobenthic biomass hotspots and associated benthivory in the Pacific Arctic. *Progress in Oceanography*, *136*, 92–114. https://doi.org/10.1016/j.pocean.2015.05.006

Grebmeier, J. M., Frey, K. E., Cooper, L. W., & Kędra, M. (2018). Trends in benthic macrofaunal populations, seasonal sea ice persistence, and bottom water temperatures in the Bering Strait region. *Oceanography*, *31*(2), 136–151. https://doi.org/10.5670/oceanog.2018.224

Hermann, A. J., Gibson, G. A., Cheng, W., Ortiz, I., Aydin, K., Wang, M., et al. (2019). Projected biophysical conditions of the Bering Sea to 2100 under multiple emission scenarios. *ICES Journal of Marine Science*, *76*(5), 1280–1304. https://doi.org/10.1093/icesjms/fsz043

Hersbach, H. (2016). *The ERA5 atmospheric reanalysis*. NG33D-01. AGU Fall Meeting Abstracts.

Hu, L., Liu, Y., Xiao, X., Gong, X., Zou, J., Bai, Y., et al. (2020). Sedimentary records of bulk organic matter and lipid biomarkers in the Bering Sea: A centennial perspective of sea-ice variability and phytoplankton community. *Marine Geology*, *429*, 106308. https://doi.org/10.1016/j.margeo.2020.106308

Huang, J., Pickart, R. S., Huang, R. X., Lin, P., Brakstad, A., & Xu, F. (2020). Sources and upstream pathways of the densest overflow water in the Nordic Seas. *Nature Communications*, *11*(1), 5389. https://doi.org/10.1038/s41467-020-19050-y

Lefebvre, K. A., Quakenbush, L., Frame, E., Huntington, K. B., Sheffield, G., Stimmelmayr, R., et al. (2016). Prevalence of algal toxins in Alaskan marine mammals foraging in a changing arctic and subarctic environment. *Harmful Algae*, *55*, 13–24. https://doi.org/10.1016/j.hal.2016.01.007

Lewis, K. M., van Dijken, G. L., & Arrigo, K. R. (2020). Changes in phytoplankton concentration now drive increased Arctic Ocean primary production. *Science*, *369*(6500), 198–202. https://doi.org/10.1126/science.aay8380

Li, Y., Stumpf, R. P., McGillicuddy, D. J., & He, R. (2020). Dynamics of an intense *Alexandrium catenella* red tide in the Gulf of Maine: Satellite observations and numerical modeling. *Harmful Algae*, *99*, 101927. https://doi.org/10.1016/j.hal.2020.101927

Lin, P., Pickart, R. S., Heorton, H., Tsamados, M., Itoh, M., & Kikuchi, T. (2023). Recent state transition of the Arctic Ocean's Beaufort Gyre. *Nature Geoscience*, *16*(6), 485–491. https://doi.org/10.1038/s41561-023-01184-5

Lin, P., Pickart, R. S., McRaven, L. T., Arrigo, K. R., Bahr, F., Lowry, K. E., et al. (2019). Water mass evolution and circulation of the northeastern Chukchi Sea in summer: Implications for nutrient distributions. *Journal of Geophysical Research: Oceans*, *124*(7), 4416–4432. https://doi.org/10.1029/2019JC015185

Lin, P., Pickart, R. S., Våge, K., & Li, J. (2021). Fate of warm Pacific water in the Arctic basin. *Geophysical Research Letters*, *48*(20), e2021GL094693. https://doi.org/10.1029/2021GL094693

Lowry, K. E., van Dijken, G. L., & Arrigo, K. R. (2014). Evidence of under-ice phytoplankton blooms in the Chukchi Sea from 1998 to 2012. *Deep-Sea Research Part II, Complete*(105), 105–117. https://doi.org/10.1016/j.dsr2.2014.03.013

Mardones, J. I., Bolch, C., Guzmán, L., Paredes, J., Varela, D., & Hallegraeff, G. M. (2016). Role of resting cysts in Chilean *Alexandrium catenella* dinoflagellate blooms revisited. *Harmful Algae*, *55*, 238–249. https://doi.org/10.1016/j.hal.2016.03.020

Muench, R. D., Schumacher, J. D., & Salo, S. A. (1988). Winter currents and hydrographic conditions on the northern central Bering Sea shelf. *Journal of Geophysical Research*, *93*(C1), 516–526. https://doi.org/10.1029/JC093iC01p00516

Natsuike, M., Matsuno, K., Hirawake, T., Yamaguchi, A., Nishino, S., & Imai, I. (2017). Possible spreading of toxic *Alexandrium tamarense* blooms on the Chukchi Sea shelf with the inflow of Pacific summer water due to climatic warming. *Harmful Algae*, *61*, 80–86. https://doi.org/10.1016/j.hal.2016.11.019

Natsuike, M., Nagai, S., Matsuno, K., Saito, R., Tsukazaki, C., Yamaguchi, A., & Imai, I. (2013). Abundance and distribution of toxic *Alexandrium tamarense* resting cysts in the sediments of the Chukchi Sea and the eastern Bering Sea. *Harmful Algae*, *27*, 52–59. https://doi.org/10.1016/j.hal.2013.04.006

Natsuike, M., Oikawa, H., Matsuno, K., Yamaguchi, A., & Imai, I. (2017). The physiological adaptations and toxin profiles of the toxic *Alexandrium fundyense* on the eastern Bering Sea and Chukchi Sea shelves. *Harmful Algae*, *63*, 13–22. https://doi.org/10.1016/j.hal.2017.01.001

Olson, R. J., & Sosik, H. M. (2007). A submersible imaging-in-flow instrument to analyze nano-and microplankton: Imaging FlowCytobot. *Limnology and Oceanography: Methods*, *5*(6), 195–203. https://doi.org/10.4319/lom.2007.5.195

Orlova, T. Y., & Morozova, T. V. (2019). Dinoflagellate cysts of the genus Alexandrium Halim, 1960 (Dinophyceae: Gonyaulacales) in recent sediments from the northwestern Pacific ocean. *Russian Journal of Marine Biology*, *45*(6), 397–407. https://doi.org/10.1134/S1063074019060075

Pacini, A., Moore, G. W. K., Pickart, R. S., Nobre, C., Bahr, F., Våge, K., & Arrigo, K. R. (2019). Characteristics and transformation of Pacific winter water on the Chukchi Sea shelf in late spring. *Journal of Geophysical Research: Oceans*, *124*(10), 7153–7177. https://doi.org/10.1029/2019JC015261

Padman, L., & Erofeeva, S. (2004). A barotropic inverse tidal model for the Arctic Ocean. *Geophysical Research Letters*, *31*(2), L02303. https://doi.org/10.1029/2003GL019003

Paquette, R., & Bourke, R. (1974). Observations on the coastal current of Arctic Alaska. *Journal of Marine Research*, *32*(2). https://elischolar.library.yale.edu/journal_of_marine_research/1286

Pickart, R. S., Lin, P., Bahr, F., McRaven, L. T., Huang, J., Pacini, A., et al. (2023). The Pacific water flow branches in the eastern Chukchi Sea. *Progress in Oceanography*, *219*, 103169. https://doi.org/10.1016/j.pocean.2023.103169

Pickart, R. S., Pratt, L. J., Torres, D. J., Whitledge, T. E., Proshutinsky, A. Y., Aagaard, K., et al. (2010). Evolution and dynamics of the flow through Herald Canyon in the western Chukchi Sea. *Deep Sea Research Part II: Topical Studies in Oceanography*, *57*(1), 5–26. https://doi.org/10.1016/j.dsr2.2009.08.002

Pickart, R. S., Spall, M. A., Bahr, F., Lago, L., Lin, P., Pacini, A., et al. (2024). Vertical carbon export during a phytoplankton bloom in the Chukchi Sea: Physical setting and frontal subduction. *Journal of Geophysical Research: Oceans*, *129*(11), e2024JC021465. https://doi.org/10.1029/2024JC021465

Pisareva, M. N., Pickart, R. S., Spall, M. A., Nobre, C., Torres, D. J., Moore, G. W. K., & Whitledge, T. E. (2015). Flow of pacific water in the western Chukchi Sea: Results from the 2009 RUSALCA expedition. *Deep Sea Research Part I: Oceanographic Research Papers*, *105*, 53–73. https://doi.org/10.1016/j.dsr.2015.08.011

Proenca, L. a. O., & Hallegraeff, G. (2017). *Marine and fresh-water harmful algae: Proceedings of the 17th International conference on Harmful Algae*. University of Tasmania. Retrieved from https://figshare.utas.edu.au/articles/conference_contribution/Marine_and_Fresh-water_Harmful_Algae_Proceedings_of_the_17th_International_Conference_on_Harmful_Algae/23157869/1

Ralston, D. K., Brosnahan, M. L., Fox, S. E., Lee, K. D., & Anderson, D. M. (2015). Temperature and residence time controls on an estuarine harmful algal bloom: Modeling hydrodynamics and Alexandrium fundyense in Nauset Estuary. *Estuaries and Coasts*, *38*(6), 2240–2258. https://doi.org/10.1007/s12237-015-9949-z

Shearn-Bochsler, V., Lance, E. W., Corcoran, R., Piatt, J., Bodenstein, B., Frame, E., & Lawonn, J. (2014). Fatal paralytic shellfish poisoning in Kittlitz's Murrelet (Brachyramphus brevirostris) Nestlings, Alaska, USA. *Journal of Wildlife Diseases*, *50*(4), 933–937. https://doi.org/10.7589/2013-11-296

Solow, A. R., Beet, A. R., Keafer, B. A., & Anderson, D. M. (2014). Testing for simple structure in a spatial time series with an application to the distribution of Alexandrium resting cysts in the Gulf of Maine. *Marine Ecology Progress Series*, *501*, 291–296. https://doi.org/10.3354/meps10705

Stabeno, P. J., & Bell, S. W. (2019). Extreme conditions in the Bering Sea (2017–2018): Record-breaking low sea-ice extent. *Geophysical Research Letters*, *46*(15), 8952–8959. https://doi.org/10.1029/2019GL083816

Stabeno, P. J., Thoman, R. L., & Wood, K. (2019). Recent warming in the Bering Sea and its impact on the ecosystem. NOAA Tech. Rep. (pp. 81–87). Retrieved from https://arctic.noaa.gov/Portals/7/ArcticReportCard/Documents/ArcticReport-Card_full_report2019.pdf

Stigebrandt, A. (1984). The North Pacific: A global-scale estuary. *Journal of Physical Oceanography*, *14*(2), 464–470. https://doi.org/10.1175/1520-0485(1984)014<0464:TNPAGS>2.0.CO;2

Tachibana, Y., Komatsu, K. K., Alexeev, V. A., Cai, L., & Ando, Y. (2019). Warm hole in Pacific Arctic sea ice cover forced mid-latitude Northern Hemisphere cooling during winter 2017–18. *Scientific Reports*, *9*(1), 5567. https://doi.org/10.1038/s41598-019-41682-4

Tian, F., Pickart, R. S., Lin, P., Pacini, A., Moore, G. W. K., Stabeno, P., et al. (2021). Mean and seasonal circulation of the eastern Chukchi Sea from moored timeseries in 2013–2014. *Journal of Geophysical Research: Oceans*, *126*(5), e2020JC016863. https://doi.org/10.1029/2020jc016863

Weingartner, T., Aagaard, K., Woodgate, R., Danielson, S., Sasaki, Y., & Cavalieri, D. (2005). Circulation on the north central Chukchi Sea shelf. *Deep Sea Research Part II: Topical Studies in Oceanography*, *52*(24–26), 3150–3174. https://doi.org/10.1016/j.dsr2.2005.10.015

Weingartner, T. J., Cavalieri, D. J., Aagaard, K., & Sasaki, Y. (1998). Circulation, dense water formation, and outflow on the northeast Chukchi Shelf. *Journal of Geophysical Research*, *103*(C4), 7647–7661. https://doi.org/10.1029/98JC00374

Wilks, D. S. (2011). *Statistical methods in the atmospheric sciences*. Academic Press.

Wood, K. R., Bond, N. A., Danielson, S. L., Overland, J. E., Salo, S. A., Stabeno, P. J., & Whitefield, J. (2015). A decade of environmental change in the Pacific Arctic region. *Progress in Oceanography*, *136*, 12–31. https://doi.org/10.1016/j.pocean.2015.05.005

Woodgate, R. A. (2018). Increases in the Pacific inflow to the Arctic from 1990 to 2015, and insights into seasonal trends and driving mechanisms from year-round Bering Strait mooring data. *Progress in Oceanography*, *160*, 124–154. https://doi.org/10.1016/j.pocean.2017.12.007

Woodgate, R. A., Aagaard, K., & Weingartner, T. J. (2005). Monthly temperature, salinity, and transport variability of the Bering Strait through flow. *Geophysical Research Letters*, *32*(4). https://doi.org/10.1029/2004GL021880

Woodgate, R. A., Weingartner, T. J., & Lindsay, R. (2012). Observed increases in Bering Strait oceanic fluxes from the Pacific to the Arctic from 2001 to 2011 and their impacts on the Arctic Ocean water column. *Geophysical Research Letters*, *39*(24). https://doi.org/10.1029/2012GL054092

Erratum

The originally published version of this article contained a typographical error. Coauthor E. Muhlbach's name was misspelled as W. Munlbach. The error has been corrected, and this may be considered the authoritative version of record.